



Pull-off Testing and Electrical Conductivity of Sn-Based Metal Powder Mixtures Cold Sprayed on Carbon Fiber-Reinforced Polymers

Andre C. Liberati¹ · Hanqing Che¹ · Panteha Fallah¹ · Phuong Vo² · Stephen Yue¹

Submitted: 24 November 2021 / in revised form: 12 April 2022 / Accepted: 12 April 2022 / Published online: 16 May 2022
© ASM International 2022

Abstract A variety of metallic powders were mixed with tin in 10:90 weight ratios and cold sprayed onto thermosetting epoxy carbon fiber-reinforced polymers (CFRPs) substrates with varying surface finishes, and onto a thermoplastic polyether-ether-ketone (PEEK)-CFRP. Where previous studies focused on understanding the impact of the secondary component (SC) on the deposition efficiency (DE) of tin, this study aims to explore the pull-off strength and electrical conductivity of the deposited coatings. An extensive study on fractured surfaces highlighted that better adhesion usually arose from increased potential to mechanically interlock with a feature at the surface such as carbon fibers or surfacing elements. The polymeric nature of the composite resin was observed to affect the pull-off strengths as the ductile thermoplastic PEEK seems to absorb more of the impinging particle energy. The pull-off strengths were then related to the SC properties, and it was observed that the better coating strengths were obtained with SC that were previously reported to be detrimental to pure Sn deposition. Finally, four-point resistivity/conductivity measurements were carried out and results were generally better than those previously reported in the literature (50–80% the conductivity of bulk tin), with variations being associated with differing bonding quality within the coatings.

Keywords adhesion testing · carbon fiber reinforced polymers · cold spray · electrically conductive coatings · metallization of polymers · mixed metal powders

✉ Andre C. Liberati
andre.liberati@mail.mcgill.ca

¹ McGill University, Montreal, Canada

² National Research Council Canada, Boucherville, Canada

Introduction

“Metallizing,” or applying metallic coatings onto polymeric substrates, has generated much interest in the past decades (Ref 1, 2), notably within the aerospace industry. Carbon fiber-reinforced polymers (CFRPs) are a material of choice for their high strength-to-weight ratios, but on the downside, the carbon fibers and epoxy resins that compose this structure are, respectively, 1,000 and 1,000,000 more times resistive than aluminum (Ref 3), thus limiting their use. As a result, there has been growing interest to develop metallized polymers and polymeric composites for structural applications (Ref 1, 4). Different technologies have been explored, such as vacuum deposition techniques (Ref 5, 6), but these methods are limited by their inability to develop thick metal coatings (over 100 μm) (Ref 7). Lay-up molding (Ref 8), wire-arc spray (Ref 9–12), flame spray (Ref 13) or air plasma spray (Ref 14, 15) have also been considered, but these techniques require high levels of thermal energy that could lead to the accumulation of residual stresses (Ref 16), oxidation of the metallic powder as well as heat damage to the substrate (Ref 17).

Cold spraying is a solid-state thermal spray process, where powder particles are accelerated by a supersonic gas jet and form a coating through plastic deformation upon impact with a substrate (Ref 18). Since it uses relatively low temperatures (several hundred degrees versus several thousand degrees for other thermal spray techniques (Ref 19), cold spray can avoid the typical issues brought by other thermal spray techniques and positions itself as a legitimate metallization approach for polymeric substrates. While cold-spraying metallic powders onto metallic substrates have been extensively explored and have provided promising results and applications (Ref 20, 21), cold-spraying metallic powders onto polymeric substrates have

provided more mixed results, mostly due to substrate erosion (Ref 22–25). In recent years, researchers have encountered some success in metallizing polymeric substrates via cold spray with a variety of metals such as tin (Ref 24, 26–28), iron (Ref 26), 316L stainless steel (Ref 29, 30), AlSi10Mg (Ref 30–32), copper (Ref 24, 26, 28, 33–35), aluminum (Ref 35) or even titanium (Ref 36). On the downside, generally reported issues included substrate damage (Ref 24, 28), relatively low deposition efficiencies (DEs) (i.e., the ratio of effectively deposited particles on the substrate versus the amount of sprayed particles) (Ref 26, 28, 29, 31), or delamination (Ref 33–35).

Several studies have tried to explain metal deposition mechanisms on polymeric substrates. In one of the earlier studies, Lupoi and O'Neill (Ref 28) noted a correlation between particle impact energy and deposition of metallic powders: Elements such as copper would lead to erosion of the substrate due to high impact energies, while soft elements such as tin and lead could deposit with some success. Ganesan et al. (Ref 23) suggested that soft powders such as tin had the possibility to deform upon impact favoring mechanical anchoring, while harder particles such as copper could not. Che et al. (Ref 24) introduced a “crack-filling” mechanism, where it was hypothesized that thermally softened or partially melted tin particles impact the substrate and, while the harder core of the particle generates microcracks in the surface epoxy, the molten part of the tin would be squeezed into these cracks and provide mechanical interlocking with the substrate. When describing the overall deposition process of metals onto polymeric substrates, they also advanced the importance of differentiating the process into two separate phases: the first-layer deposition phase (occurring between impinging metallic powders and the polymeric substrate) and the build-up phase (occurring between metallic powders and previously deposited metal powders) (Ref 26).

In the other cold-spray work, several research groups studied enhancement effects relating to the mixing of ceramic powders with metal feedstock powders: These enhancements concerned improvements in the deposition process (increased DE, decreased porosity), but also improvement of coating properties (hardness, adhesion strength between the coating and the substrate) (Ref 37–39). This led to establishing an *in situ* shot-peening cold-spray deposition process, where the same improvements are obtained through the addition of large stainless steel particles (200–300 μm) (Ref 40–42). Recently, Fernandez and Jodoin (Ref 43, 44) conducted an extensive study on potential mechanisms of improvement and explained that the coating deposition improvement is due to surface roughening by the secondary component (SC) through generation of asperities and oxide removal, while the coating property improvements are related to generation of

oxide clean surfaces and peening of the SC. When exploring the deposition of metals onto polymeric substrates with mixed metal powders, Che et al. (Ref 45) made similar observations relating to coating deposition improvement when spraying tin powders with SC such as zinc or copper, and this improvement was associated with the shot-peening effect of the SC on the relatively softer tin. Nevertheless, in recent work at McGill University (Ref 46), evidence appeared that the shot-peening effect may not be an effective mechanism when cold-spraying tin mixed with metallic powders. In a follow-up study (Ref 47), the correlation between various SC properties was explored and the deposition improvement was associated with a suitable SC hardness range, as well as a suitable SC impact energy. Nevertheless, these studies (Ref 46, 47) were mainly focused on deposition mechanisms and only briefly touched on adhesion of the coatings with the substrates.

As a matter of fact, a review of literature for cold-sprayed coatings on CFRP substrates reveals that few studies have considered adhesion strengths. This may principally be explained by the difficulty to obtain full coatings on CFRP (Ref 26, 28, 29, 31) and/or by delamination issues occurring before being able to conduct adhesion tests (Ref 33–35). It may also be explained by the relative novelty of using the cold-spray process to metallize polymeric substrates with most studies being quite recent (Ref 8, 24, 26, 27, 29–31, 33–35, 45–51), thus confirming the research community is still in the early stages of understanding how this process can be carried out efficiently. From the few studies that did report results, adhesion strengths were generally quite low. Che et al. (Ref 24) reported adhesion strengths as high as 7.6 MPa for a tin coating cold sprayed on an epoxy-CFRP. Other thermal spray results with other polymeric substrates can provide some reference as well. While cold-spraying copper onto a polyvinyl chloride (PVC) substrate, Ganesan et al. (Ref 25) obtained shear adhesion strengths below 3 MPa, and then in another study (Ref 52), they projected copper on CFRP with an atmospheric plasma spray system and recorded adhesion strengths of up to 5.4 MPa (with a tin interlayer). Małachowska et al. (Ref 53) observed similar adhesion strengths (3.6 MPa) with a low-pressure cold-sprayed copper on polyamide 6 substrates, as well as Zhou et al. (Ref 54) with aluminum coatings cold sprayed onto a PEEK-CFRP. Rezzoug et al. (Ref 12) recorded some better results when adding various CFRP interlayers before depositing zinc via wire-arc spray (up to 7 MPa): The effect of the interlayer greatly affected the adhesion strength. More recently, Che et al. (Ref 49) obtained some of the highest recorded strengths with cold-sprayed SnBi on the thermoplastic acrylonitrile butadiene styrene (ABS) (14.5 MPa versus 6.8 MPa for pure tin).

With the perspective of developing suitable coatings for potential applications in the aerospace industry, or any other field that could require polymeric substrates with thick coatings ($> 100 \mu\text{m}$), it is essential to determine the properties of cold-sprayed metallic coatings and understand inherent mechanisms that could lead toward developing a usable process. As the cold spraying of tin mixed with metallic SC powders allowed a further understanding of deposition of coatings on CFRP (Ref 46, 47), this study aims to assess the effects of these SC on some coating properties (pull-off strength and electrical conductivity) and understand how the SC may impact the adhesion of a tin coating to the CFRP.

In this study, the properties of coatings from previous studies (Ref 46, 47) are investigated. These coatings were obtained by cold-spraying tin mixed with various SCs on several CFRP substrates. The choice of SC was made to cover a wide range of SC properties (hardness, density, morphology, median particle size, and by extension impact energy), as described in (Ref 47). In both studies (Ref 46, 47), tin and tin-SC mixed powders with 90:10 weight ratio are cold sprayed with a low-pressure cold-spray system, onto thermosetting epoxy-CFRP substrates with varying surface finishes and a thermoplastic polyether-ether-ketone (PEEK)-CFRP. In this way, variability in the properties originating from the powder mixture and/or from the substrate may be observed. Pull-off strength and electrical conductivity were then evaluated, and relations between coating properties, SC and substrates were established.

Experimental Methods

Materials and Cold-Spray Conditions

The feedstock materials considered in this work were described and sprayed in previous studies (Ref 46, 47): They are summarized in Table 1. These powders were chosen to cover a variety of material properties (namely density and hardness), with a variety of morphologies and particle sizes. Powders from several studies at McGill University (Ref 45, 55–57) were chosen as SCs to offer a meaningful spread for each property. As such, the selection was made from aluminum/aluminum alloy powders from the paper (Ref 46), copper powders from studies by Che et al. (Ref 24, 45), iron and stainless steel 316L powders from studies by Chu et al. (Ref 55, 58) and titanium/Ti6Al4V powders from studies by Wong et al. (Ref 57). The properties were observed between 2.66 and $8.96 \text{ g}\cdot\text{cm}^{-3}$ for density, 7 and $340 \text{ HV}_{0.01}$ for hardness, 12 and $37 \mu\text{m}$ for median particle size (D_{50}); for the given process variables, the impact energy was between

$1.32 \cdot 10^{-6} \text{ J}$ and $7.30 \cdot 10^{-6} \text{ J}$. The characterization of the powder hardness, median particle size and average impact energy was described in (Ref 47). Powder mixtures with 90% tin and 10% of each SC powder were then mixed for 1h in a metal can without additional media (e.g., milling balls with a double movement powder mixer: This did not induce any significant morphological changes or hardening (Ref 46, 47).

The substrates used in this work were epoxy-CFRPs provided by Bombardier Aerospace (Montreal, Canada) and polyether-ether-ketone (PEEK)-CFRPs provided by TenCate (Netherlands). Top surface images of the CFRP substrates were presented elsewhere (Fig. 2 Ref 46).

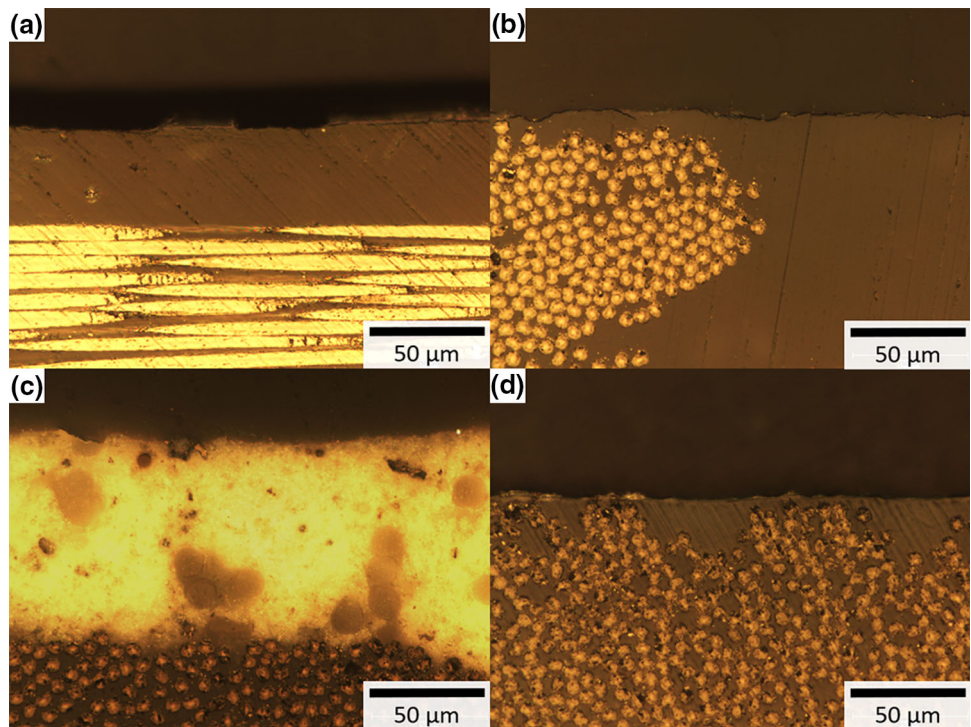
The epoxy-CFRPs (abbreviated as e-CFRP) used here consist of a thermosetting epoxy matrix with continuous carbon fiber reinforcements. The e-CFRP panels were made of four plies of epoxy/carbon fiber prepreg ($[(0/90)]_{2s}$) and have the following coating finishes used by the manufacturer: a bare finish, a putty finish and a surface film. The bare finish e-CFRP is the as-manufactured material, the putty e-CFRP has a surface filled with a pinhole filler and surfacer to produce defect-free surfaces, and the surface film e-CFRP includes a neat epoxy resin film with an embedded veil, normally a mat, at the top surface (to help handle the resin film). The cross section of these substrates was observed using a light optical microscope (LOM) and is presented in Fig. 1(a), (c). The bare e-CFRP (Fig. 1a) and putty e-CFRP (Fig. 1b) appear similar in structure, with areas rich in carbon fibers close to the top surface, and others rich in polymer close to the surface: The thickness of the putty is unclear though. Profilometric data were acquired for the raw substrates on areas of $3 \times 3 \text{ mm}$ as shown in Fig. 2 (methodology presented in next section), and the bare e-CFRP surface presents a rough, ridged surface ($S_a = 4.6 \mu\text{m}$, Fig. 2a) while the putty e-CFRP presents a smoother surface with fine inter-crossing curves ($S_a = 1.3 \mu\text{m}$, Fig. 2b). The surface film e-CFRP (Fig. 1c) presents a different cross-sectional profile with the top layer being notably different from the underlying CFRP material. While having a different top-surface appearance than the putty e-CFRP (Fig. 2 of Ref 46), these two substrates actually have similar surface textures and roughness values ($S_a = 1.6 \mu\text{m}$, Fig. 2c): As both surface finishes are destined to provide a smooth surface, the structure of inter-crossing curves may be associated with the processing step that smooths the surface. The hardness of these substrates was measured, and the values were $39 \pm 8 \text{ HV}_{0.01}$ for the bare e-CFRP, $51 \pm 15 \text{ HV}_{0.01}$ for the putty e-CFRP and $40 \pm 13 \text{ HV}_{0.01}$ for the surface film e-CFRP.

The PEEK-CFRP used here consists of a thermoplastic polyether-ether-ketone matrix with continuous carbon fiber reinforcements. These panels were made of five plies of PEEK/carbon fiber ($[(0,90)_2/(0,90)_3R]$). The cross section

Table 1 Properties of the feedstock powders considered in this work

References	Powder	Morphology	Supplier	D ₅₀ , μm	Hardness, HV _{0.01}	Density, g.cm ⁻³	Average kinetic energy, J (Ref 47)
(Ref 46)	Sn	Spheroidal	Center line	12	7±1	7.29	2.28.10 ⁻⁶
	Al	Spherical	Valimet	23	24±2	2.70	2.09.10 ⁻⁶
	Al5083	Spherical	Valimet	17	66±11	2.66	1.62.10 ⁻⁶
	Al6061	Spherical	Valimet	23	72±8	2.70	2.62.10 ⁻⁶
	Al7075	Spherical	Valimet	20	118±23	2.81	1.96.10 ⁻⁶
(Ref 47)	Sn	Spheroidal	Center line	13	8±1	7.29	1.32.10 ⁻⁶
	Cu	Mixed	Giken	30	68±7	8.96	5.19.10 ⁻⁶
	Cu-IR	Dendritic	Center line	33	32±4	8.96	6.88.10 ⁻⁶
	Fe	Mixed/IR	Goodfellow	37	89±14	7.87	7.30.10 ⁻⁶
	SS316L	Spherical	Sandvik	23	215±26	8.00	2.84.10 ⁻⁶
	Ti-SP	Spherical	Raymor (AP&C)	20	196±22	4.50	1.58.10 ⁻⁶
	Ti-AG	Angular	Cerac	30	178±34	4.50	4.36.10 ⁻⁶
	Ti6Al4V	Spherical	Raymor (AP&C)	37	340±14	4.43	4.56.10 ⁻⁶

Fig. 1 Optical images of the substrate cross sections, near the top-surface: (a) bare e-CFRP, (b) putty e-CFRP, (c) surface film e-CFRP, (d) PEEK-CFRP



of this substrate is presented in Fig. 1d. Its structure is fairly similar to that of the bare e-CFRP (Fig. 1a) in such that the substrate has an as-manufactured finish, with areas where the carbon fibers are close to the top surface versus other areas where the polymer is close to the surface, as well as a ridged surface, presumably with intertwining carbon fiber structures, as seen in Fig. 2 (d): The Sa roughness of this substrate is measured at 2.9 μm. The hardness of this substrate was differentiated between areas showing superficially pure PEEK areas and superficially

predominant carbon fiber areas. The respective hardness values for each area are 26±3 HV_{0.01} and 63±22 HV_{0.01}.

Sheet sections of dimensions 7 cm × 7 cm × 1.7 mm were used as substrates during the cold-spray campaigns. The substrates were degreased with ethanol before cold spraying, but they were not grit-blasted as it would result in the erosion of the substrate.

The cold spraying was performed at the McGill-NRC cold-spray facility at National Research Council Canada in Boucherville and was also presented in previous studies

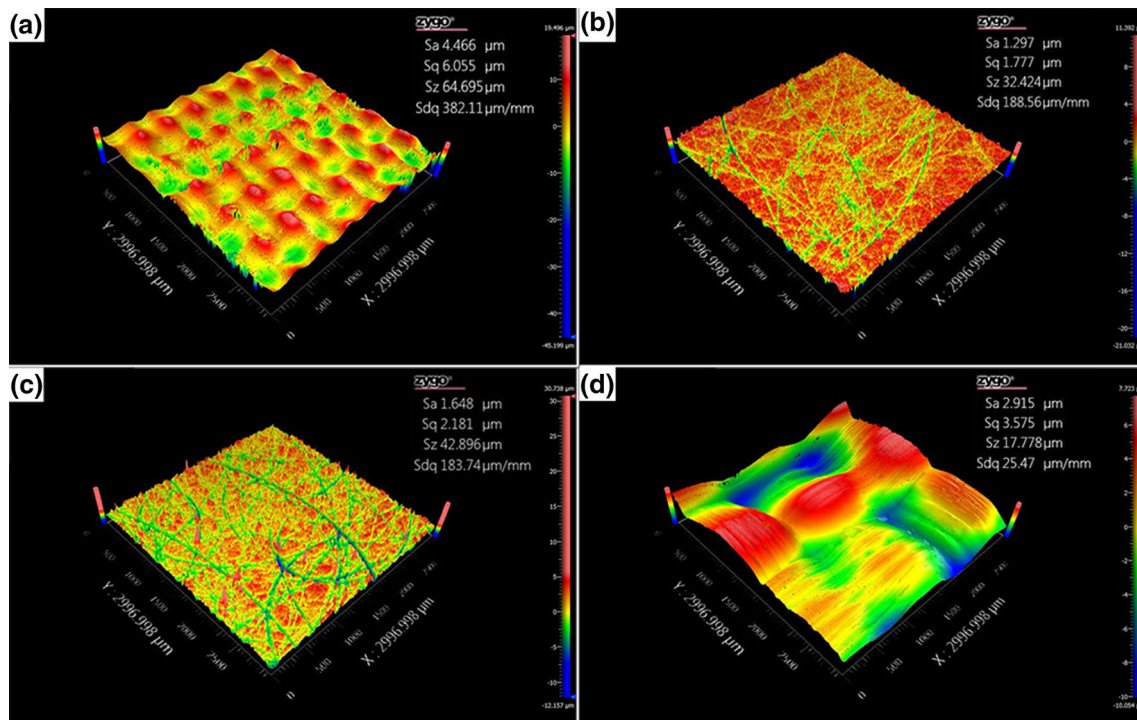


Fig. 2 Height profiles of the as-received substrates at 2,75x: (a) bare e-CFRP, (b) putty e-CFRP, (c) surface film e-CFRP, (d) PEEK-CFRP

(Ref 46, 47). The cold spraying was performed at low pressure with a commercially available CenterLine SST SSM-P3300 system (Supersonic Spray Technologies, CenterLine Windsor Limited, Canada). Pure tin powder, or powder mixtures with 90% tin and 10% of each SC powder, was cold sprayed onto each substrate with gas conditions of 310 °C and 60 psi (0.41 MPa). These parameters were chosen based on previously successful cold spray campaigns with tin (Ref 24, 27, 45–47, 49, 51); at the selected conditions, melting was observed in previous work (Ref 24, 27, 45, 49, 51). A comparison between cold-spraying pure tin and the powder mixtures with SCs of varying properties was thus possible, on a variety of CFRP substrates. The carrier gas was nitrogen, the standoff distance was 18 mm, the step size was 1 mm with 38 steps, and the gun travel speed was 25 mm/s. The powder feeder rate was between 9.9 and 16.9 g/min, measured every three sprays to accurately assess the variation. The substrates were pre-heated by operating a single pass, without powder injection. Then, only one pass was sprayed for each set of conditions, so that the results provided from spraying on a large area, together with a study focused more on the behavior of the process than the numerical results, would be meaningful. All the substrates were aligned and sprayed at the same time for one condition, so that any external variation (e.g., feeding, temperature effects) may be neglected.

Coating Properties and Characterization

The pull-off strength was measured by means of pull-off tests performed on all tin and tin-SC-coated CFRP samples. The testing was modified based on the ASTM C-633-01 standard and required cutting the cold-sprayed samples (Delta Abrasimet, Buehler, Illinois, USA) into specimens measuring approximately $1.5 \times 1.5 \text{ cm}^2$. The coating surfaces were slightly ground in order to remove loose particles from the cold-spray process, and then these surfaces were glued to a 60-grit pre-ground Al6061 cylinder with a room temperature curing adhesive. The choice of this adhesive was made to have a high glue strength without requiring thermal treatment, as tin has a low melting point and the curing process could affect the coating before testing. The substrate surfaces were also glued to another 60-grit pre-ground Al6061 cylinders. The pull-off tests were performed using an MTS hydraulic pressure machine at a constant crosshead speed of 1.0 mm/min. For each coating, three tests were performed, and the average strength was taken. The glue strength was determined as the average strength for which coatings would not peel from the substrate and breaking of the glue would occur: This value was found to be around 13 MPa. This would also indicate that coatings with indicated strengths above 13 MPa may actually be higher due to the glue breaking.

The samples were then taken, and the fracture surfaces were characterized with a Keyence (Japan) digital

microscope and a Hitachi (Japan) SU3500 scanning electron microscope. A 3D optical surface profiler (ZYGO, Connecticut, USA) was also used to measure the surface roughness and support large-scale microstructural observations. The lateral resolution of the objectives used is below 2 μm . The main measurements were taken around the roughness S_a , the peak-to-valley height S_z and the root-mean-square gradient of the surface S_dq as they provide insight into the topography of the surfaces regarding not only height but also gradient (Ref 59, 60). More specifically, S_dq is affected both by texture amplitude and spacing; therefore, S_dq can provide information on the slopes which comprise the surface in the case of coatings with similar values of S_a (Ref 60). This metric was successfully used to correlate surface changes in another study (Ref 51).

The electrical conductivity measurements were conducted at École Polytechnique de Montréal (Montréal, Québec, Canada) by using the four-point resistivity/conductivity measurement method (Ref 45, 48, 61). Before the measurements, the as-sprayed top surfaces were slightly ground to remove loose particles and obtain flat surfaces for measurement. For each sample, the measurements were taken at three different locations, and the average value was taken. The linearity of the conductivity was verified by taking measurements at 100 and 50 mA.

Results

Pull-off Test Results

The pull-off strength of the various deposited coatings from (Ref 46, 47) is presented in Fig. 3: The glue adhesion strength was determined to be 13 MPa and is indicated on each graph for reference. The results vary notably between both studies (cf. Sn (Ref 46) and Sn (Ref 47)) so it is important to observe the effects of the SC as compared to their respective pure Sn coatings. During the pull-off test, the coatings mostly peeled at the interface and presented adhesive failure. In some instances, mixed cohesive/adhesive failure was observed and areas with Sn could be observed on the substrate surface.

On the bare e-CFRP, the pull-off tests either led to failure of the coating at the substrate interface (with SC Al/Al alloys, Cu, Cu-IR) or the glue failed before peeling of the coating occurred (with SC Fe, SS316L, Ti-SP, Ti-AG, Ti6Al4V) (Fig. 3a). For the coatings deposited in the first study (Ref 46), the addition of Al or Al alloys to Sn led to a decrease of the coating pull-off strength by 2–5 times that of single component Sn (from 7.9 to 1.7–4.4 MPa). For the Sn deposited on the bare e-CFRP in the second study (Ref 47), notably better strengths were obtained (coatings mostly did not peel). The addition of Fe, SS316L or any of

the Ti/Ti6Al4V powders did not noticeably decrease the strength of the Sn on the bare e-CFRP, as all strengths remained above 13 MPa: These results are actually higher than those reported in the literature for metallic coatings deposited onto polymeric substrates (Ref 12, 24, 25, 49, 52–54). On the other hand, the addition of Cu, and, to a lesser extent, Cu-IR, led to lower strengths compared to the pure Sn coating that did not peel (respectively, 3.7 and 9.4 MPa).

A similar graph profile may be observed between the bare e-CFRP and putty e-CFRP for the pull-off strength of the cold-sprayed coatings (Fig. 3b). One notable difference is that strengths were generally lower for the putty e-CFRP and that glue failure never occurred (strengths < 10MPa). As with the bare e-CFRP, the addition of Al and Al alloys to Sn resulted in lower strengths as compared to the Sn coating sprayed in (Ref 46) (from 4.7 to 1.1–2.2 MPa). The Sn coatings sprayed in the second study (Ref 47) showed an average strength of 8.2 MPa on the putty e-CFRP. The addition of Fe/SS316L slightly increased that value (8.5 and 9.2 MPa, respectively), while the addition of Ti-SP, Ti-AG and Ti6Al4V led to slight decreases (6.3–7.4 MPa). For this substrate, the addition of Cu and Cu-IR had the effect of reducing the strength by more than half (3.7–4.1 MPa).

The pull-off strengths on the surface film e-CFRP (Fig. 3c) showed a very different profile compared to the other e-CFRP substrates, as the coatings provided overall better strengths with an average of 9.5 MPa across all the sprayed powders. The Sn coatings from the first study (Ref 46) had a strength of 13.1MPa, and while the addition of Al/Al alloys again led to a decrease in pull-off strength, this decrease was quite uneven with Al5083 providing the lowest strength (3.9 MPa), while Al provided a strength of 8.8 MPa. For coatings in the second study (Ref 47), strengths were above 8.4 MPa, with some notable variation (standard deviation above 2 MPa for most powders). In this situation, and given the indicated errors, there does not seem to be noticeable variation of the pull-off strength when adding the various SC, apart from Ti6Al4V that produces a coating with a high strength of 13.0 MPa.

The pull-off strength on the PEEK-CFRP provided the lowest strengths of this study (Fig. 3d). When adding Al alloys to feedstock Sn powder (Ref 46), peeling was an issue during sample preparation, which made it impossible to measure an effective strength for these coatings (except for Al). For the coatings sprayed in the second study (Ref 47), there were no issues of peeling during sample preparation, and strengths were observed to be between 2.8 and 5.2 MPa for most coatings. Two noticeable results appeared here with Cu-IR providing relatively lower strength (1.0MPa), while Ti6Al4V provided relatively higher strength (8.2 MPa).

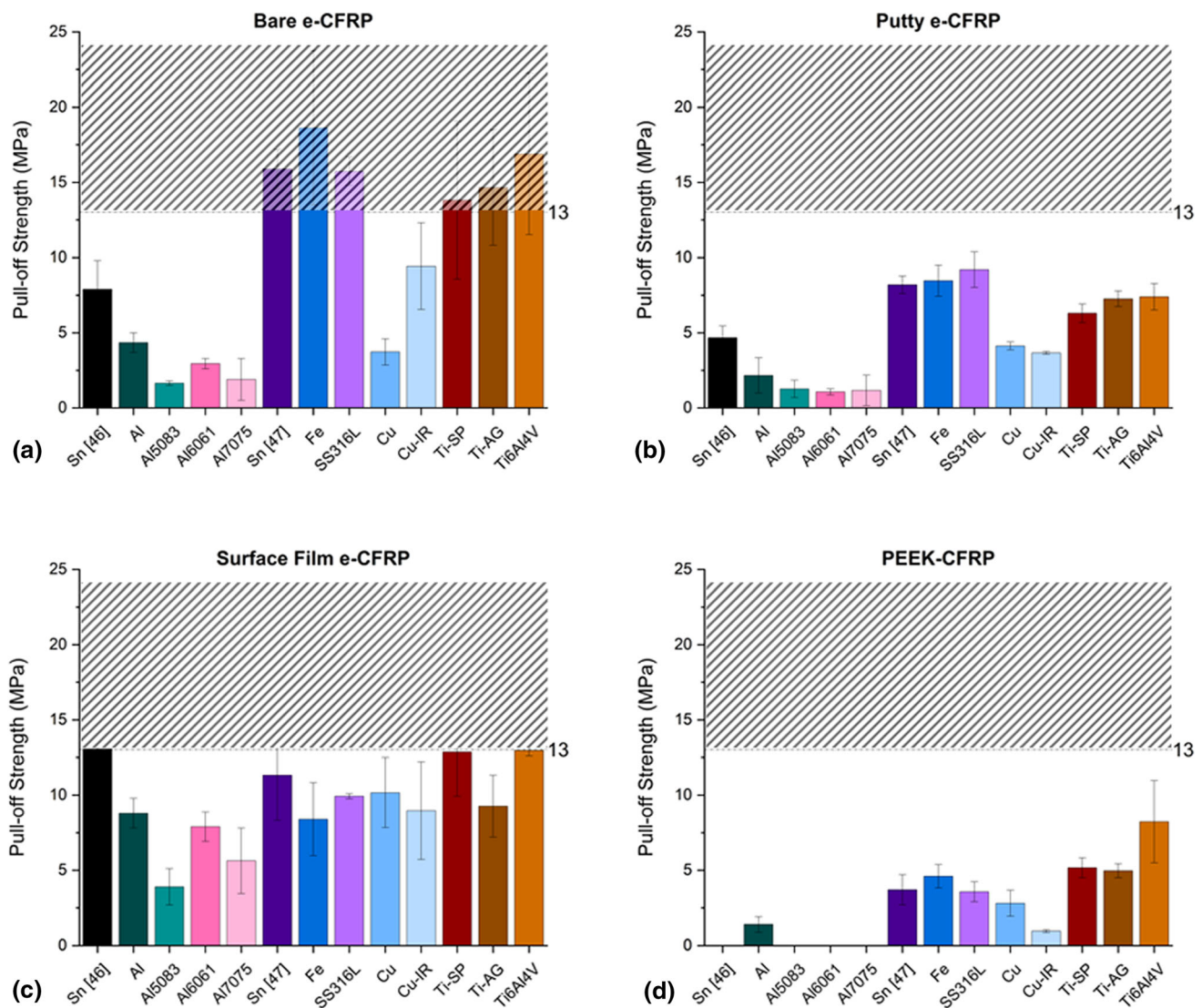


Fig. 3 Pull-off strength of the Sn and Sn-SC powder mixtures on the various CFRP substrates: (a) bare e-CFRP, (b) putty e-CFRP, (c) surface film e-CFRP, (d) PEEK-CFRP. The values provided are

the average of three measurements, and values above 13 MPa are representative of the glue failure

Characterization of Fracture Surfaces

Bare e-CFRP

Images of tested coatings on bare e-CFRP substrate are presented in Fig. 4. An example of the substrate side of the fracture is presented in Fig. 4a, and several areas of interest can be noted. In the middle of the image, lines can be seen on the surface and are representative of carbon fibers near the surface. The epoxy appears to be roughened all over the surface. The light gray regions spread throughout the substrate are remnants of tin still bonded with the substrate after peeling of the coating. These tin remnants were generally more frequently found in areas with visible carbon fibers. When conducting SEM of the substrate side,

exposure of the carbon fibers did not appear clearly but some carbon fibers were nevertheless observed, as shown by the linear structures in the middle of Fig. 4(b). Around these areas, accumulations of tin powders were also noted: Some powder-like shapes could be observed, but a general structure in these mounds was unclear. Furthermore, linear tin structures could be observed around the carbon fibers. When observing the coating side (Fig. 4c), several other structures were observed: Around the edge of the image, a flat tin surface corresponding to the interface of the coating/substrate was observed, while in the center of the image, the interior of the coating could be observed with apparent powder-like structures. When using SC Cu-IR, more mounds of tin were observed on the substrate, and larger areas of the interior of the coating could be observed.

In BSE images of the coating side, a high proportion of darker contrast particles could be observed: These are Cu-IR particles as copper has a lower atomic number than tin and therefore generates darker contrasts (Fig. 4d).

Putty e-CFRP

Images of tested coatings on putty e-CFRP substrate are presented in Fig. 5 and 6. An example of the substrate side of the fracture is presented in Fig. 5(a). Striated structures, attributed to the carbon fibers of the substrate, are visible among a somewhat homogeneous structure which would be attributed to the epoxy or pinhole filler at the top surface of the substrate. An example of coating cross section before testing is presented in Fig. 5(b), and bonding of tin around the carbon fibers (circular structures of the lower half) can

be noted before the test was conducted. In Fig. 6(a), the substrate side of the tested coating shows an homogeneous linear structure that is the carbon fibers of the substrate. The top and bottom edges of this image reveal a dark structure that covers the carbon fibers, and this is the epoxy polymer. Finally, bright linear areas seem to border the carbon fibers or some of the epoxy on the substrate. This would be tin from the peeled coating, but there is no specific morphology associated with it. In areas with mostly superficial polymer (Fig. 6b), a very heterogeneous and roughened structure is observed. In this area, tin also seems to be present, with some local points of accumulation, but it is important to notice the scale of the image and that these points are quite small, and without any apparent structure. The coating side of an area matching the carbon fibers of the substrate is presented in Fig. 6(c). The

Fig. 4 (a) Keyence digital microscope image of the substrate side of a tested Sn-10Cu coating on bare e-CFRP. (b) SEM image of the substrate side of a tested Sn-10Cu-IR coating on bare e-CFRP. (c) SEM image of the coating side of a tested Sn-10Al5083 coating on bare e-CFRP, which showed mixed cohesive/adhesive failure. (d) SEM BSE-COMP image of the coating side of a tested Sn-10Cu-IR coating on bare e-CFRP, which showed mostly cohesive failure: The darker contrast is Cu-IR

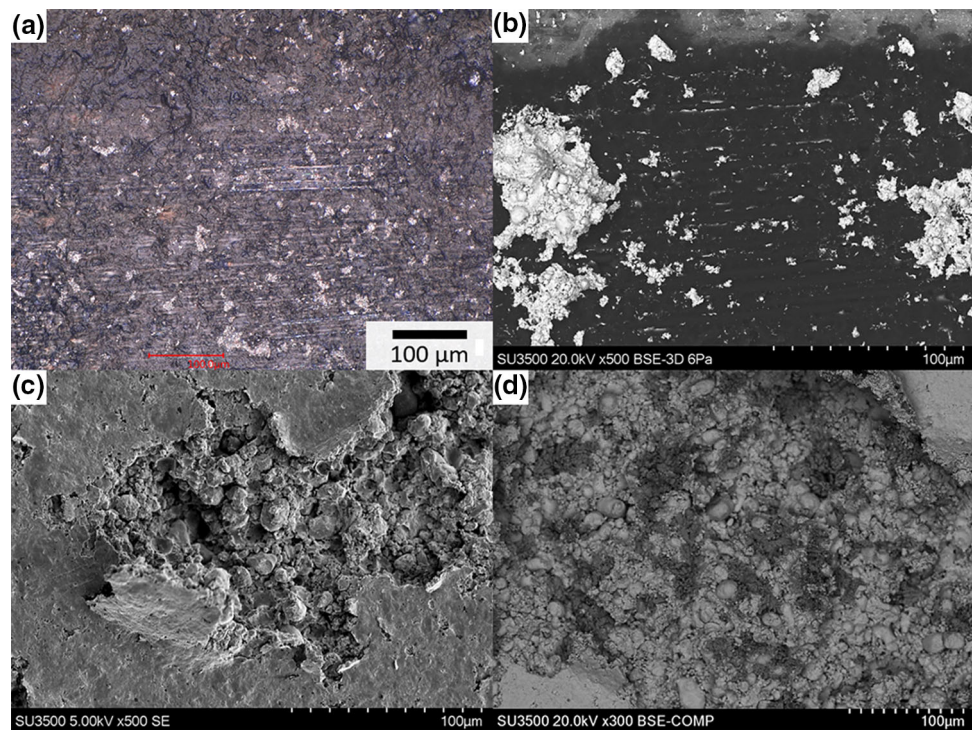


Fig. 5 (a) Keyence digital microscope image of the substrate side of a tested Sn-10Ti6Al4V coating on putty e-CFRP substrate. (b) Optical image of the cross section of a pure Sn (Ref 47) coating on the putty e-CFRP substrate, at the coating/substrate interface

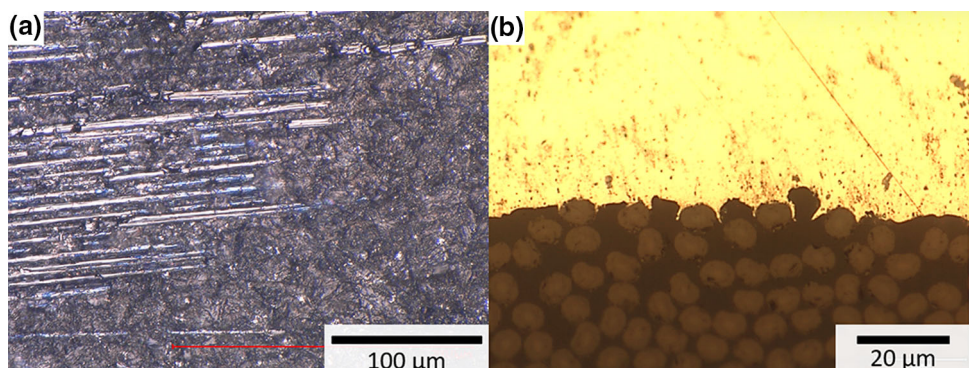
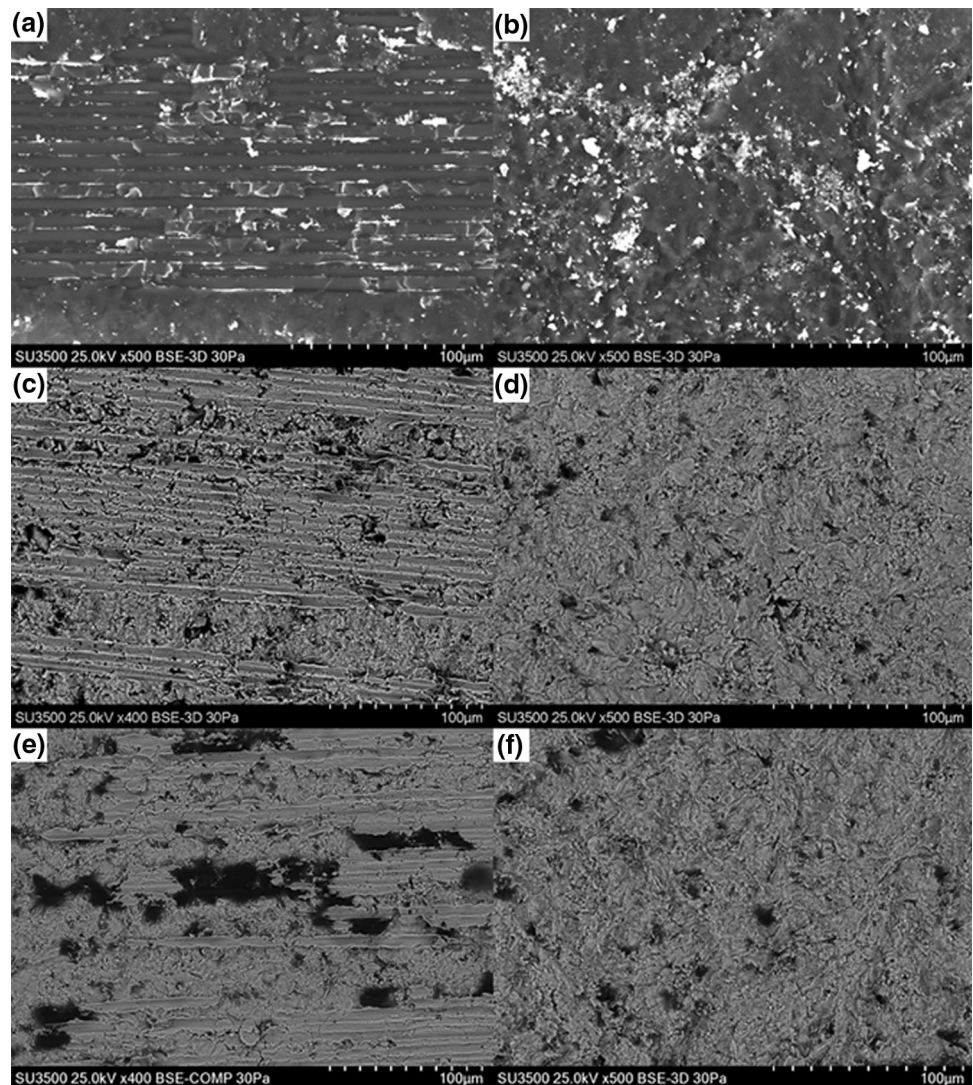


Fig. 6 SEM images of tested coatings on putty e-CFRP: (a) substrate side of a tested Sn-10SS316L coating and (b) substrate side of a tested Sn-10Al coating. (c) and (d) are, respectively, the coating side of tested Sn-10Cu-IR and Sn-10Al coatings. (e) and (f) are the coating side of tested Sn-SS316L coatings



structure of this coating seems complementary to the carbon fibers of the substrate with long grooves, but these are discontinuous, and it seems that tin particles can be discerned within the grooves. On the coating side of an area matching the polymeric area (Fig. 6d), a wavelike structure of tin particles can be observed, and this seems complementary to the topography observed on the substrate side (Fig. 6b). For the sake of comparison, the coating side of a tested Sn-10SS316L coating is presented in Fig. 6(e), (f). In Fig. 6(e), more continuity is observed in the long grooves and tin particles are less discernable. Large voids are also present which could be related to removal of sections of the coating during testing. On the other hand, the polymeric area of the same coating (Fig. 6 f) presents a similar profile to that described in Fig. 6(d).

Surface Film e-CFRP

When characterizing the substrate surface, a heterogeneous fracture surface was obtained (Fig. 7a): Micron-sized spherical particles were observed to be embedded in the top surface of the substrate, with rings of highly contrasted elements (tin) surrounding them. Besides these particles, a roughened structure was present, similar to what was observed on the polymer area of the putty e-CFRP (Fig. 6b). Some large areas of tin were also observed on this coating (bright features of Fig. 7b). Some grayish features, indicated by white arrows, can be observed in this area of bright contrast and they correspond to Cu-IR particles. The aforementioned spherical particles are also observed in the polymer, again, surrounded by rings of tin. On the coating side, spherical craters can be observed (Fig. 7c) and they appear to be complementary to the particles observed on the substrate surface. Around these

craters, the structure of the tin particles seems to adopt a wavelike structure (Fig. 7c), comparable to that of the putty e-CFRP (Fig. 6d). Finally, with tin accumulations being present on the substrate for the SC Cu-IR coating (Fig. 7b), it was possible to observe the interior of the peeled coating: Tin particles (lighter contrast) were clearly visible, and a large number of Cu-IR particles were present.

PEEK-CFRP

Images of tested coatings on PEEK e-CFRP substrate are presented in Fig. 8 and 9. In Fig. 8, initially similar areas with superficial carbon fibers were considered: The light blue structure (edges of Fig. 8a, b) is the PEEK polymer, and the linear structure of the center is the carbon fibers. A degree of discontinuity can be observed in the carbon fiber area with the tested pure Sn coating in Fig. 8(a), while the

carbon fiber area seems larger and more damaged with the addition of SC Ti6Al4V in Fig. 8(b). No idea of roughness in the polymer is apparent here (as it was for the bare e-CFRP in Fig. 4a), but this is due to the lower magnification. What is noticeable though, is the degree of roughening of the carbon fiber areas at this lower magnification. Some bright elements appear within the carbon fiber area, and these could be remnants of tin or reflections of light on damaged polymer/carbon fibers. Further characterization of these areas is conducted in Fig. 9. The carbon fiber area of a tested pure Sn coating is shown in Fig. 9(a), and several carbon fibers (vertical tubes) can be observed. These carbon fibers are partially covered by dark features that are the PEEK polymer. Furthermore, some highly contrasted linear features are present between the delimitations of the PEEK polymer and the carbon fibers, and this would be tin. Around the carbon fiber area, a slightly cratered polymer

Fig. 7 SEM images of tested coatings on surface film e-CFRP: (a) substrate side of a tested Sn-10Al coating and (b) substrate side of a tested Sn-10Cu-IR coating. (c) and (d) are, respectively, the coating side of tested Sn-10Al and Sn-10Cu-IR coatings. (b) and (d) are BSE-COMP images and the darker contrast of powder areas is Cu-IR

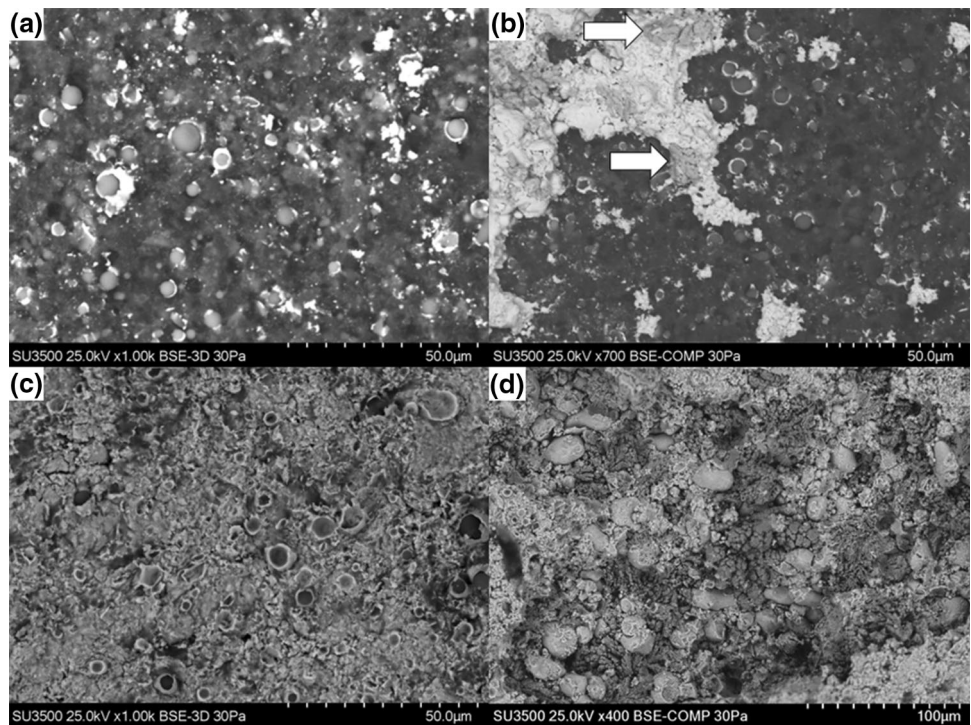


Fig. 8 Keyence digital microscope image of the superficial carbon fiber area on the substrate side of tested coatings on PEEK-CFRP: (a) Sn (Ref 47), (b) Sn-10Ti6Al4V

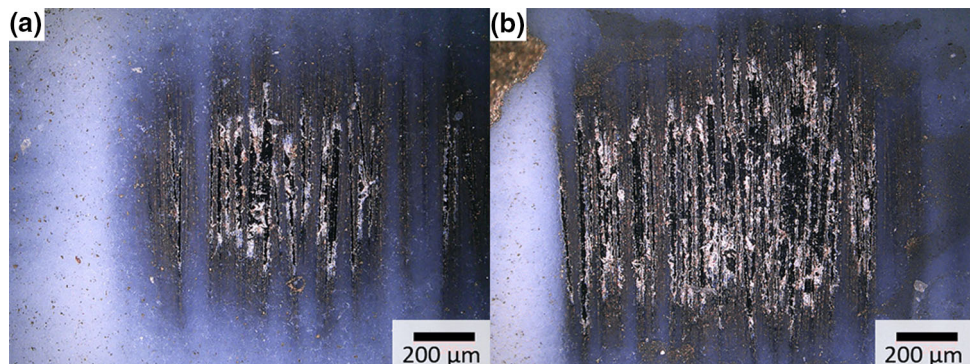
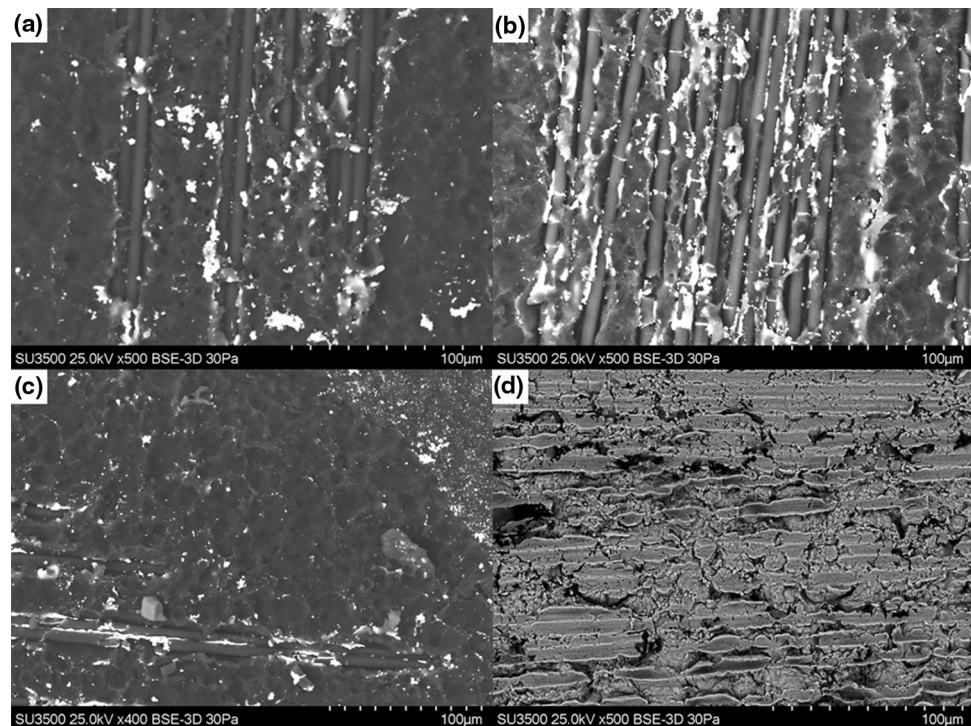


Fig. 9 SEM images of tested coatings on PEEK-CFRP: (a) substrate side of a tested Sn (Ref 47) coating, (b, c) substrate side of a tested Sn-10Ti6Al4V substrate, (d) coating side of a tested Sn-10Ti6Al4V coating



structure seems to appear. In Fig. 9(b), a similar substrate area of a tested Sn-10Ti6Al4V coating is presented: The image is slightly brighter, but the carbon fibers appear far more clearly. The area around these carbon fibers also appears more cratered. Further consideration is given to the area around the carbon fibers in Fig. 9(c), and a cratered structure is more obvious. Linear bright features seem to predominantly appear around the carbon fiber area, but not so much in the cratered area. Finally, the coating side of the tested Sn-10Ti6Al4V coating is observed in Fig. 9(d): The coating is complementary to the carbon fibers of the substrate with long grooves, but these appear quite discontinuous, and tin particles can be made out within the grooves.

Comparison of Pull-off Strength and SC Properties

While the previous section mostly focused on fracture surfaces for the various substrates, the SC may also play a role in the variation of coating strengths. In past studies, the importance of SC hardness (Ref 46, 47) and SC impact energy (Ref 47) appeared to be the key factors that affected DE and will therefore be considered here. In the first section, it also appeared that the bare e-CFRP, putty e-CFRP and PEEK-CFRP provided similar trends with the Al and Cu powders providing coatings with lower strengths than pure Sn, and with the Fe and Ti-based powders providing similar or better strengths (Fig. 3). The putty e-CFRP and the PEEK-CFRP showed lower average strengths than the

bare e-CFRP (Fig. 3), and the bare e-CFRP showed more contrast in the strength values than the other substrates. As a result, focus will be put on the relation between the SC properties and the pull-off strengths on the bare e-CFRP in this section, but the trends that are described are similar for the putty e-CFRP and the PEEK-CFRP.

The pull-off strengths from the bare e-CFRP, as a function of SC impact energy and SC hardness, are presented in Fig. 10. It appears that SC with low hardness and any value of impact energy lead to pull-off strengths lower than their tin counterpart: SC Al/Al alloy lead to strengths below 5 MPa, while Sn (Ref 46) has a strength above 5 MPa, and SC Cu/Cu-IR lead to strengths below 10 MPa, while the glue broke when testing Sn (Ref 47). It should be noted that SC Cu-IR nevertheless led to a higher pull-off strength than the other SC Al and Cu powders, and Cu-IR had the highest average impact energy. For the SC with higher hardness, and any impact energy (Fe and Ti-based SC), the glue almost always broke during the testing which would indicate that they may provide pull-off strengths on par or better than pure Sn (Ref 47).

Height profiles of $827 \times 827 \mu\text{m}$ areas were taken on the bare e-CFRP substrate for substrates that had peeled (Fig. 11), and roughness measurements were taken to study a potential relation between the substrate surface roughness and the pull-off strengths of the coatings. The as-manufactured substrate (Fig. 11a) naturally has lower roughness (S_a), peak-to-valley height (S_z) root-mean-square gradient (S_{dq}) than the substrates after removal of the coatings

Fig. 10 Pull-off strength on the bare e-CFRP for the various SCs, represented as a function of the SC hardness and impact energy

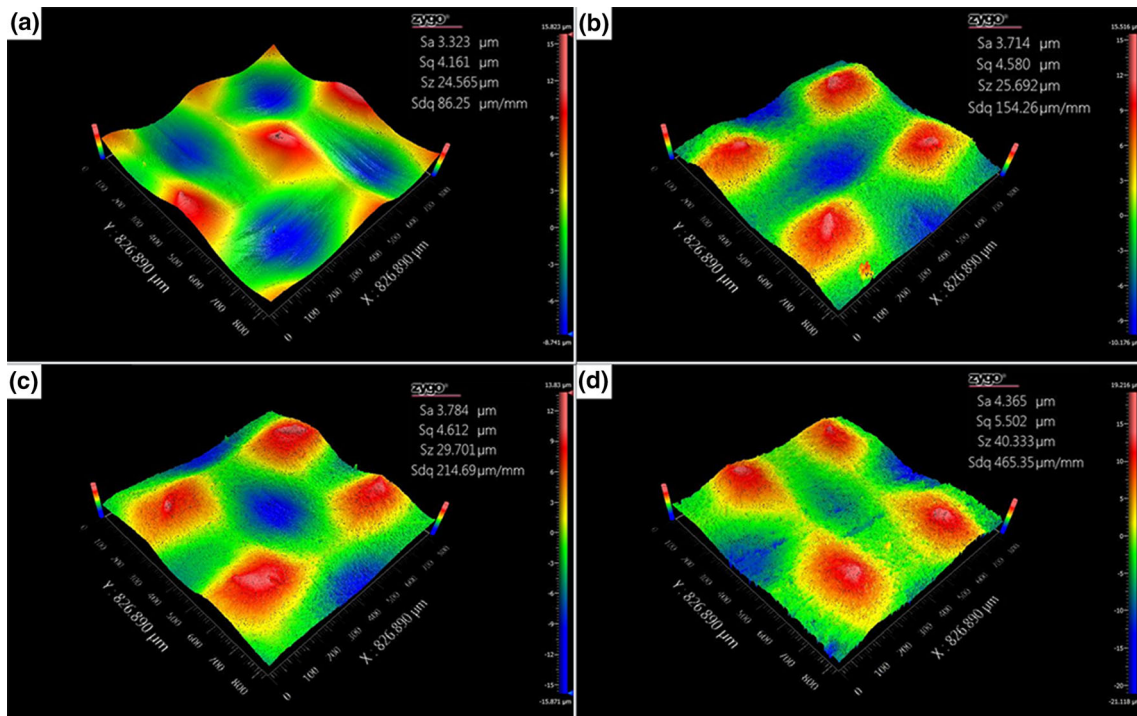
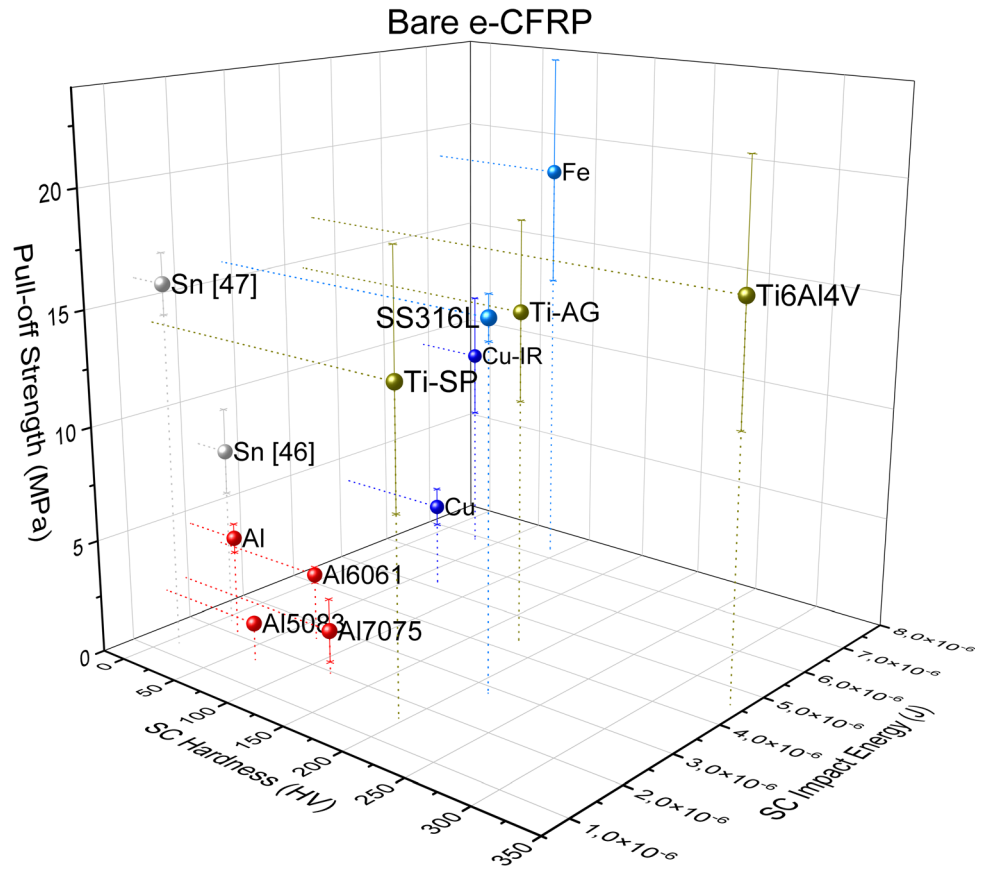


Fig. 11 Height profiles of a bare e-CFRP substrate at 10x: (a) as-received, (b) after peeling of a Sn (Ref 46) coating, (c) after peeling of a Sn-10Al5083 coating, (d) after peeling of a Sn-10SS316L coating

(Fig. 11b-d). After removal of the pure tin coating, increases of each of these parameters are observed, with a near doubling of S_{dq} from 86 to 154 $\mu\text{m}/\text{mm}$ (Fig. 11b). With the addition of SC to the powder mixture (Fig. 11c, d), these increases were even higher with SC SS316L providing values of S_{dq} over 5 times that of the as-manufactured bare e-CFRP and 3 times higher than the substrate surface after removal of the pure Sn coating.

Electrical Conductivity

Electrical conductivity measurements were conducted on all substrates and are presented in Fig. 12. Generally, conductivities between 50 and 80% of the conductivity of pure Sn (9.10^6 S/m) are obtained. In some circumstances, the electrical conductivity was very low and generated high standard deviations (Sn (Ref 46) on the surface film

e-CFRP or on the PEEK-CFRP, Sn-10Ti6Al4V on the PEEK-CFRP), but this could be associated with the “poor” or discontinuous aspect of these coatings (Ref 46, 47).

Discussion

Adhesion of Coatings to CFRP

The main features observed in the characterization of the fracture surfaces were carbon fibers, polymer areas, and highly contrasted tin areas. These tin areas appeared under two forms: mounds of tin or linear structures. All these areas could vary in shape and size: Typically, the carbon fibers would be more or less apparent, while the polymer area would appear more or less roughened. Finally, the tin mounds would be larger than the size of several particles

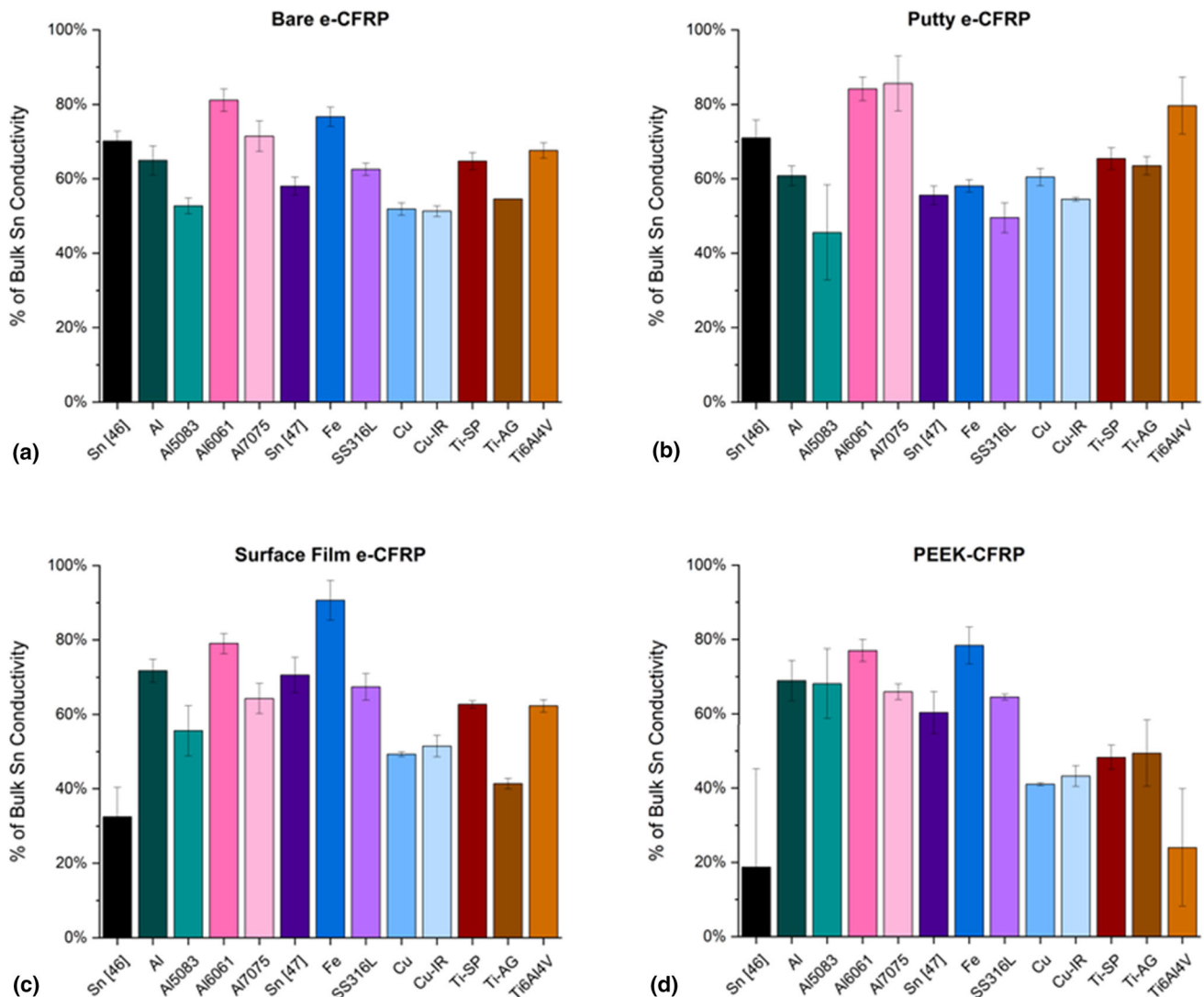


Fig. 12 Electrical conductivity of the various Sn and Sn-SC powder mixtures, on the various CFRP substrates: (a) bare e-CFRP, (b) putty e-CFRP, (c) surface film e-CFRP, (d) PEEK-CFRP. The conductivity is expressed as a percentage of Bulk Sn conductivity (9.10^6 S/m)

(>10 μm), while the linear structures of tin would be smaller (<10 μm). The following section discusses a potential correlation between fracture surfaces and pull-off strengths based on the observation of these features.

Bare e-CFRP

The presence of tin mounds at the surface of the bare e-CFRP substrate (Fig. 4a-b) and the observation of the interior of the coating after the pull-off test (Fig. 4c-d) would indicate that the debonding is not purely adhesive and that some cohesive component should be included. The epoxy is quite roughened on the substrate (Fig. 4a) and could provide some retention, but the tin at the substrate/coating interface (Fig. 4c) is highly deformed (flattened) so there seems to be little or no means of mechanical interlocking with the substrate in these areas. This would then suggest that the bonding of the coating with the substrate must occur in areas where the cohesive failure occurs. Furthermore, the small linear tin structures along the carbon fibers (Fig. 4b) have no specific structure and are very small in size: These may only be remnants from tin melting during the spraying process (Ref 24, 27, 45, 49, 51) and may not be elements of the coating. With tin being accumulated and quite deformed around the carbon fiber area (Fig. 4b), it could then be suggested that the bonding of the coating intimately depends on the bonding with the carbon fiber area and that more deformation (i.e., mechanical interlocking) can occur here. These results support conclusions of previous work (Ref 46, 47), where it was suggested that deposition would occur in the superficial carbon area and that these areas would be prime for occurrence of the “crack-filling” mechanism.

The role of the SC is more difficult to explain: In some situations (with SC Fe, SS316L, Ti-SP, Ti-AG, Ti6Al4V), the coatings did not peel from the substrate, while other SC (Al/Al alloys, Cu/Cu-IR) led to relatively lower strengths than pure tin (Fig. 3). The SC is hypothesized to generate surface roughness (on the substrate or on the coating) and peening of the coating (during the build-up phase) (Ref 43, 44). The SC is harder and generally has higher kinetic (i.e., impact) energies than the tin particles (Table 1), so they should have higher potential for “crack generation” at the substrate interface (Ref 46, 47) and therefore provide improved anchoring of tin to the substrate. More bonding of tin with the substrate would be expected and observed either through more areas of revealed carbon fibers (if adhesive strength is the limiting factor) or more areas of tin on the substrate side (if cohesive strength is the limiting factor). The tin particles within the observed coatings do not seem very deformed for SC Al5083 (Fig. 4c) and SC Cu-IR (Fig. 4d) as their morphology is comparable to the

initial feedstock powder (Fig. 1a of (Ref 46)) or Fig. 2a of (Ref 47)), so the involved SC may not provide notable peening, and bonding may be relatively poor when compared to the relatively higher bonding occurring at interfaces with carbon fibers. It is possible that these SC generates greater adhesive strength for the coating, but their presence in the coating (albeit sometimes very low (Ref 47)) leads to more cohesive failure, and overall lower pull-off strengths than the pure Sn coatings. Typically, a large distribution of Cu-IR particles was observed in the back of the peeled coating (Fig. 4d), and these particles were not as present in the areas of cohesive failure on the substrate side (Fig. 4b): This could reinforce the idea that these SC bond poorly with Sn and weaken the pull-off strength. As for the addition of other SC (Fe/SS316L, Ti/Ti6Al4V), peeling did not occur much like the Sn coating: It is possible that these SC helped with the crack-filling mechanism and/or provided better cohesive bonding, potentially through improved peening of the coating.

Putty e-CFRP

On the putty e-CFRP substrate, no mounds of tin were observed and the coatings always peeled due to adhesive failure. Tin was present around the carbon fibers before testing (Fig. 5b), the carbon fiber areas were well exposed after testing (Fig. 5a and Fig. 6a), and tin grooves on the coating side of tested coatings were observed, so it would seem that mechanical anchoring appears in the carbon fiber area. A contribution of anchoring from the deformed tin in roughened epoxy areas seems possible as well (Fig. 6b, d), but given the large difference in pull-off strength between Sn-10Al and Sn-10SS316L (Fig. 3) and the relatively similar structure in this area for these coatings (Fig. 6d, f), this does not seem very likely. Some linear tin structures were observed on the substrate side after fracture (Fig. 6a-b) and probably do not have a role in coating adhesion. Nevertheless, while the bonding seems related to the carbon fiber area for this substrate, the strengths for all coatings are actually lower than on the bare e-CFRP (Fig. 3). Given the attribution of “good adhesion” to carbon fiber areas for the bare e-CFRP, the absence of tin mounds (cohesive failure) and the clear exposure of the carbon fiber areas should also be explained.

The nature of bonding with metal/polymer (or metal/composite) systems is still not entirely understood (with only the “crack-filling” as a point of reference (Ref 24)), but some observed elements may explain the differences with the bare e-CFRP. A first element of comparison would naturally be the surface finish of each substrate: With its as-manufactured finish, the bare e-CFRP is slightly rougher than the putty e-CFRP (Fig. 2a, b) which could be associated with better potential for mechanical

interlocking. While this would be a traditional metric to consider for metallic substrates, the bonding process has been hypothesized to occur in the carbon fiber area in the case of CFRP, i.e., after removal of some surface polymer layer, therefore it is uncertain if the initial surface roughness affects deposition to a noticeable extent. Furthermore, it is possible that some carbon fiber areas (those at the bottom of the valleys of Fig. 2(a)) are covered by the pinhole filler in the putty finish on the e-CFRP, therefore cutting in half the number of areas the coating could efficiently bond to. This pinhole filler would have a polymeric nature (i.e., little or no contribution to mechanical interlocking) and could also partially cover carbon fiber areas near the peaks of the holes, reducing the area that tin could bond to. Therefore, regardless the quality of bonding observed in the carbon fiber area, the overall load of the peel-off test would be applied to a lower number of areas (i.e., higher local strain), and ultimately, the coating would show lower strength.

Another element to differentiate the widely varying pull-off strengths between substrates could be the observation of tin particles on the backside of the coatings with cracks or voids between the particles (Fig. 6c). This could indicate less uniformity and qualitatively less deformation of the tin impacting the substrate, when compared with tested coatings on the bare e-CFRP that had very uniform coating interfaces (Fig. 4c): This could then lead to weaker bonding of the coating and, as a result, poorer mechanical interlocking with the substrate. This idea would be supported by the comparison between the observed carbon fiber area of the Sn-10Cu-IR (Fig. 6c) and Sn-10SS316L tested coatings (Fig. 6e), where the latter shows more continuous deformation of particle and within the grooves and also shows notably higher pull-off strengths (Fig. 3). Therefore, with seemingly less adhesive coatings in the carbon fiber areas and less areas to adhere to, the putty e-CFRPs would provide lower strengths than the bare e-CFRP. A direct consequence of weaker bonding would also be that the coating would present adhesive failure before any cohesive failure, which would explain the absence of tin mounds on this substrate, and any carbon fibers that would have been covered with tin mounds on the e-CFRP would be revealed due to the adhesive failure of the putty e-CFRP. Since the coatings with the highest strengths did not peel, it is nevertheless difficult to confirm if the bonding around the carbon fibers of the bare e-CFRP was on a large area (comparable to the putty e-CFRP).

Surface film e-CFRP

With an average pull-off strength of 9.5 MPa, the strengths of coatings on the surface film e-CFRP compare as better than most reported results in the literature (Ref

12, 24, 25, 49, 52–54). While carbon fiber structures were observed on tested coatings on bare e-CFRP and putty e-CFRP, the surface film e-CFRP coatings provided notably different observations: Carbon fiber areas were never observed and cross-section observations of these coatings (not presented here) confirm that the cold-sprayed particles are not in contact with the carbon fibers. Only micron-sized spherical particles with rings of tin appeared on the substrate side (Fig. 7a, b). These micron-sized particle seem to originate from the preparation of the substrate, as they could already be distinguished in the top layer of Fig. 1(c). The rings of tin around these particles could be remnants of melted tin (Fig. 7a-b) that appeared during the spray process, similar to the local tin tracks on the bare and putty e-CFRPs (Fig. 6a-b): It is possible that their role for bonding is also negligible. Some coatings such as tin with SC Cu-IR left accumulations of tin at the surface (Fig. 7b), indicating that debonding on this substrate was due to mixed adhesive/cohesive failure. Since it was quite unclear if the roughened structure of the putty e-CFRP (Fig. 6b, d) would portray mechanical interlocking of tin in the polymeric substrate area, it would seem that the bonding of the coatings to the surface film e-CFRP substrate is related to the bonding of the tin to the spherical particles at the top surface of the substrate. In light of the high deformation of tin particles around these spherical elements (craters of Fig. 7c) and the high average coating strength (Fig. 3c), it could be suggested that this bonding is relatively strong. These spherical particles also seem heterogeneous in size and in distribution on the top surface of the substrate (Fig. 7a-b) which could explain the strong variability observed for the bonding results (Fig. 3c). Furthermore, the observation of the cross sections of surface film e-CFRP coatings, presented in Fig. 5 of (Ref 46) and Fig. 6 of (Ref 47), seems to reveal a more roughened interfacial area than the cross sections of bare or putty e-CFRP coatings presented in (Ref 45), and this interfacial roughness could also be related to increased overall pull-off strength. Nevertheless, this one-dimensional feature is difficult to characterize and would be best addressed by measuring the roughness of the fracture surfaces.

Finally, as with the bare e-CFRP, it seems Cu-IR led to some local cohesive failure with areas remaining bonded to the substrate (top left corner of Fig. 7b): These areas are mostly tin with some Cu-IR particles. The coating side of the corresponding sample also presents tin particles with little deformation as compared to the initial feedstock powder, as well as a high proportion of Cu-IR (Fig. 7d). A combination between a hypothesized local increase of spherical particles (that would increase adhesion due to strong bonding) and a cohesive failure due to poor bonding between the tin and Cu-IR could explain how these structures are obtained.

PEEK-CFRP

Pull-off strengths for the PEEK-CFRP substrate presented a similar trend to those observed for the bare e-CFRP and the putty e-CFRP. As for the putty e-CFRP, no notable accumulation of tin was observed on the PEEK-CFRP substrate suggesting that all coatings on this substrate present adhesive failure. Through the observation of craters in the polymer area (Fig. 9c), it could be suggested that peening of the PEEK polymer appears and little/no mechanical interlocking can occur here, as previously suggested (Ref 46). This cratering appears in contrast to a roughened structure that was observed for the putty and surface film e-CFRPs (Fig. 6d and Fig. 7c). The phenomenon could be related to the different polymeric nature of the substrate: PEEK being a thermoplastic material, it could be subjected to thermal softening and deformation, while the thermosetting epoxy in previous substrates would be directly subjected to cracking, fracture and/or erosion.

Again, it would then seem that the bonding of the coatings is related to the mechanical interlocking of tin in the carbon fiber area of the substrate. Similar carbon fiber areas were observed for pure Sn (Fig. 8a and Fig. 9a) and for Sn-10Ti6Al4V (Fig. 8b and Fig. 9b), and it appeared that SC Ti6Al4V revealed the carbon fibers more, as the areas were larger, the fibers appeared more clearly and less polymer seemed present. The strength of this coating was also notably higher than the strength of the pure Sn coating (8.2 MPa compared to 3.7 MPa, Fig. 3d). Furthermore, the peeled coating of Sn (Ref 46), which was studied in Fig. 8 of (Ref 46), seems to reveal relatively less visible carbon fibers than compared to what is observed in Fig. 9 in this work, hinting toward lower peel-off strength (without providing an actual value given this coating had peeled before testing). This information could prove to be quite valuable as previous studies suggested the SC could generate more surface roughening and catalyze the “crack-filling” mechanism on CFRP substrates (Ref 46, 47), but past observation never revealed notable difference between coatings that could support this theory, and the observation of the e-CFRPs did not provide results that could fully support this hypothesis. While this could explain the improvement of bonding between the pure Sn and Sn-10Ti6Al4V coatings, SEM observations of the substrate from the peeled Sn-10Cu-IR coatings (not presented here) revealed a profile similar to that of the pure Sn (Fig. 8a), while having a lower adhesion strength (1.0MPa); therefore, systematic analysis of the substrates after testing would need to be conducted to confirm if there is a relation between the area of revealed carbon fibers and the obtained strength.

Even though the structure of the PEEK-CFRP was close to that of the bare e-CFRP (as-manufactured finish), the

PEEK-CFRP led to the lowest pull-off strengths of this work. Where putty e-CFRP had a structural difference that could explain the decrease in pull-off strengths (pinhole filler), the lower results with PEEK-CFRP seem related to the nature of the substrate. As previously mentioned, the thermoplastic polymer is subject to ductile deformations, whereas thermosets are not, and so the bonding of the coating with the substrate may be worse, notably due to dissipation of the particle deformation energy in the substrate. This could be confirmed by the discontinuous grooves of Fig. 9(d) where different particles are discernable, even more so than in the coating of the bare (Fig. 4c) and putty e-CFRPs (Fig. 6d). This lack of coating uniformity and lesser deformation of tin particles at the substrate interface seems more important than for the putty e-CFRP and could therefore also explain why overall lower strengths are observed on the PEEK-CFRP, as compared to the bare and putty e-CFRPs.

Summary

Based on the pull-off test results and fracture surface observations for each substrate, the following points can be made:

- The bare e-CFRP provided some of the highest pull-off strengths of this study with many coatings not peeling (Fig. 3a). This would be related to high levels of deformation of the tin at the coating/substrate interface (Fig. 4c), and good bonding in the carbon fiber area. Bonding was related to cohesive and adhesive elements, and the presence of some SC in the coating seemed to present a weakening effect on the coating strength.
- The putty e-CFRP pull-off strengths showed a similar trend to the bare e-CFRP, albeit with lower values (Fig. 3b). Bonding in the carbon fiber area was notably clearer (Fig. 5a), but this seemed to be offset by the surface finish that removed half of the carbon fiber areas that the coating could bond to (areas that would be at the bottom of the filled pinholes, or the valleys of Fig. 2 (a))
- The surface film e-CFRP provided overall good coating strengths (Fig. 3c) and this was related with a different surface finish, comprised of micro-sized spherical particles embedded in the polymer at the surface of the substrate (Fig. 7 a-b). The tin seems to greatly deform around these particles, leading to good bonding, and their heterogeneous distribution would explain the variation in strength measurements.
- The PEEK-CFRP provided the weakest coatings of this work (Fig. 3d), and this was mostly associated with the different substrate nature (thermoplastic versus

thermoelastic, for epoxy). Of notable interest, it appeared that the presence of the SC generated increased presence of carbon fibers at the surface of the substrate, which could explain the increase between pure Sn and the coating with SC Ti6Al4V.

From the obtained results, it would then seem that better adhesion was obtained when 1) a high level of tin deformation was observed at the coating/substrate interface, and 2) tin had a feature that it could bond with (carbon fiber or spherical particles of the surface film e-CFRP). These results complement cross-sectional characterization that was carried out in previous studies (Ref 24, 45–47), where one-dimensional observation of interfacial areas would only reveal a degree of roughened surface that may depend on the substrate (bare or putty e-CFRP presented in (Ref 24, 45) versus surface film e-CFRP presented in (Ref 46, 47) or clear mechanical interlocking of Sn around carbon fibers, as shown in Fig. 5(b). The variety of obtained results highlights the importance of the surface finish, as Rezzoug et al. (Ref 12) had suggested in their study with wire-arc sprayed zinc on various interlayers on CFRP.

Influence of the Sn and SC Powders on the Pull-off Strength

As mentioned in the description of the pull-off test results (Fig. 3 and 10), the pull-off strengths vary notably between the coatings of Sn (Ref 46) and Sn (Ref 47), so it is important to observe the effects of the SC as compared to their respective pure Sn coatings. The pull-off strengths of Sn (Ref 46) are notably lower than those for Sn (Ref 47) when considering the bare e-CFRP, putty e-CFRP and PEEK-CFRP, but not the surface film e-CFRP, which seems to denote some correlation between the coating adhesion and the type of substrate. It would then seem that in the case of coatings bonding to substrates with apparent carbon fiber areas (Fig. 4, 6 and 9), Sn (Ref 46) seems less prone to efficient mechanical interlocking, and mostly adhesive failure is observed. One notable difference in the properties of these powders is the difference in modeled kinetic energy (Table 1, established in (Ref 47): Sn (Ref 46) had higher kinetic energy than Sn (Ref 47), and this would be relatable to a higher value of D_{90} used for Sn (Ref 46) (33.7 μm) versus the value of D_{90} considered for Sn (Ref 47). Nevertheless, while higher kinetic energy would potentially lead to a higher proportion of potentially erosive particles as determined in (Ref 47) (11% for Sn (Ref 46)) versus 8% for Sn (Ref 47), this would only really affect deposition and would not seem to correlate with the bonding of tin to the coating. Another difference that could then explain why Sn (Ref 46) offers less efficient bonding

and lower pull-off strengths than Sn (Ref 47) could then be a difference in oxide layer thickness: Presuming that Sn (Ref 46) has a higher oxide layer thickness, it would then be more difficult for this powder to deform and mechanically interlock with the carbon fiber areas of the concerned substrates, while Sn (Ref 47) could have a thinner oxide layer which would facilitate powder deposition on the various substrates. Oxide layer thickness was not specifically studied here, and the hardness between both Sn powders does not seem to noticeably vary, so this hypothesis would require further confirmation.

By differentiating the SC properties, it appears more clearly that the decrease in strength related to the addition of Al/Al alloys to Sn in (Ref 46) would be related to SC with low hardness and low impact energy (Fig. 10). In (Ref 47), these SC provided the highest increases in pure Sn DE and this range of powder properties was described as ideal for powder deposition: In light of these results, it would then seem that improved DE compares with a decrease in pull-off strength, as can be seen in Fig. 13. The Al/Al alloy particles were described as having a hardness and an impact energy that would be sufficient to generate cracks that the tin could then fill (Ref 47), but as much as the deposition process may be catalyzed with these conditions, the bonding seems worse. Since Sn also has low hardness and similar impact energy, the difference could then be explained by the presence of Al/Al alloy in the coating, as explained for the bare e-CFRP. Given the chosen cold-spray parameters (i.e., low velocities) and observations in another study (Ref 50), it is likely that Al is not bonding with the Sn in the coating and only being retained by mechanical interlocking. The retention rate of Al/Al alloys

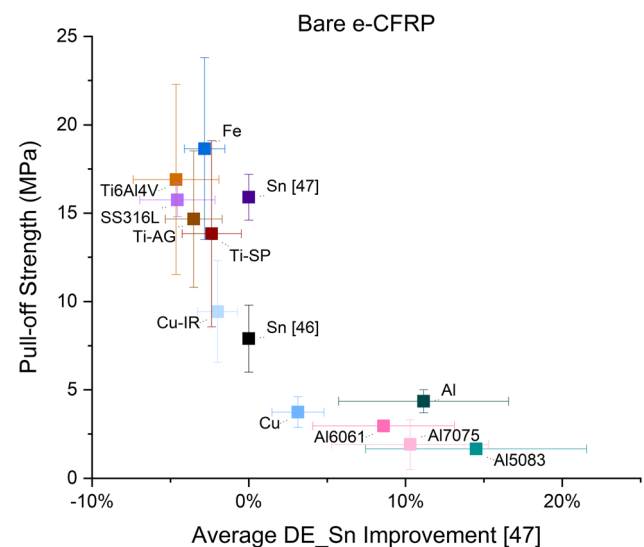


Fig. 13 Pull-off strength of the Sn and Sn-SC powder mixtures on the bare e-CFRP substrate, as a function of the average pure Sn DE improvement (Ref 47)

was low (below 1% (Ref 46)) and the distribution of particles seems somewhat random (Fig. 5 of (Ref 46)), but if an analogy is taken with the coordination number of a close packed structure, one particle could affect a dozen neighboring particles (depending on size of the particles, etc.), so even a low percentage of retained Al/Al alloy particles in the coating could still act as a contaminant for the bonding of the coating.

Fe- and Ti-based SCs led to decreases in the DE of pure Sn onto the CFRP, and this was associated with higher impact energies and/or hardnesses that led to more erosion of the coating during the build-up phase (Ref 47). From the perspective of strengths, these SC from (Ref 47) provided values on par, or slightly better, than the Sn powder they were sprayed with on the bare e-CFRP, but also on the putty e-CFRP and on the PEEK-CFRP (Fig. 10). Their hardness is higher than the hardness of the substrates (above 180 HV_{0.01}, except for Fe), and their impact energy covers the range of energies considered for all powders. This supports the idea that the hardness of the SC is the key factor in maintaining or improving the pull-off strength of the coatings. While SC Fe has a hardness of 89 HV_{0.01} (lower than that of Al7075), it also has the highest average impact energy of this study ($7.3 \cdot 10^{-6}$ J). SC Cu and Cu-IR have low hardness values (on par with SC Al and Al alloys), but higher and increasing impact energy. Figure 10 suggests that with increasing impact energy at lower hardness values, the pull-off strength increases. This idea would then suggest that the SC impact energy has a second-order effect behind SC hardness. Therefore, high hardness (and/or high impact energy) would be required to obtain good bonding on CFRP. This result is not entirely new as metallic surfaces are generally grit-blasted with hard particles (such as alumina) with the objective of enhancing adhesion strength (Ref 62), but from the perspective of composite materials where grit blasting leads to erosion of the substrate, this in-situ blasting by the SC on the CFRP could provide softer conditions that generate enhanced properties. Again, these trends are opposite to those observed for the DE of pure Sn, as high hardness (and/or high impact energies) would lead to lower pure Sn DE (Ref 47) (Fig. 13). The mechanism explaining the opposing trends would be the same as for SC with high hardness and/or impact energy: They would have higher potential of roughening the surface and generating cracks that the tin could then fill to mechanically bond with the substrate, as seen for the PEEK-CFRP in Fig. 8. In conclusion, it would then seem that the pure Sn DE improvement mechanism discussed in previous studies (Ref 46, 47) would come at the expense of the pull-off strength of the coating.

The role of the SC on the surface film e-CFRP had not yet been discussed, yet the trend seems more difficult to

describe for this substrate. The bonding mechanism seems related to the presence of spherical particles at the top surface of the substrate (Fig. 7a-b) and high variability is observed for the strength of the various powder mixtures (Fig. 3), which could suggest that the effect of the SC for this coating is not as relevant as it may have been for the other CFRPs, where a strong component of the bonding mechanism came from crack-generation mainly around the carbon fiber area.

When looking at the roughness data of Fig. 11, the results seem to indicate that the addition of an SC leads to more surface roughening, which would support the idea that the SC could catalyze the deposition of tin onto CFRP (as discussed in (Ref 46, 47)). Nevertheless, correlations between the various roughness parameters, SC and coating strengths did not reveal clear trends that could explain the variations of strength. This assessment was also limited by the absence of peeling for the coatings that provided the highest strengths (with Fe- and Ti-based SC). More systematic analysis of the coatings would be required to determine the precise mechanisms at play (roughening of the surface by the SC or peening of the substrate/coating) to understand how the bonding occurs and what processing or powder factors may influence it.

Electrical Conductivity

Differentiating the electrical conductivity results is a difficult task as there seems to be few common trends (Fig. 12). From the perspective of the substrates, the average conductivities are not noticeably different, so the substrate does not appear to affect this property, as it may have affected the pull-off strengths (Fig. 3). The SC does not seem to provide a trend either: Although having similar hardness and impact energies, the addition of Al/Al alloy to pure Sn can have both positive effects (Al6061/Al7075) and negative effects (Al/Al5083) on the coating conductivity. The retention of Al in these coatings is always low (below 1%) (Ref 46) so retention of the SC should not noticeably affect the conductivity, while SC Fe, and to a lesser extent SS316L, provides better coating conductivity than pure Sn, regardless of higher retention rates (3-5% (Ref 47) that could act as a contaminant. Finally, the conductivity of coatings with SC Al/Al alloys was found to be generally on par or greater than those with SC Cu (Fig. 12), while Cu is known to have a higher conductivity than Al, given its naturally passivated state.

While the variations may be difficult to understand, these conductivity results could be indicative of the bonding of the tin in the coating, as better bonding of the particles and less porosity (through increased plastic deformation) should lead to conductivities closer to those of the bulk material. However, plastic deformation would

also lead to more dislocations in the particles, which could hinder electrical conductivity, and compete with the improvements provided by decreased porosity. Furthermore, the relation between conductivity and bonding quality could be supported by the cohesive failure that was observed for some coatings, such as Sn-10Al5083 on bare e-CFRP (Fig. 4 c), Sn-10Cu-IR on bare e-CFRP (Fig. 4d) or Sn-10Cu-IR on surface film e-CFRP (Fig. 7d), as these coatings tend to present lower electrical conductivities than the other coatings (around 50%) (Fig. 12). As a result, while the mechanism is uncertain (competing effects), the SC would seem to affect the coating conductivity via its impact on Sn in the coating. It is also possible that the SC may affect the conductivity via its retention in the coating (such as Cu-IR, ~ 20%wt. (Ref 47)) as higher retention rates were shown to lead to lower conductivities in a previous study, presumably due to an increasing number of interfaces which could act as barriers to electron movement (Ref 45). To some extent, SC oxide layer thickness could also lead to limiting the movement of electrons, which could also explain the differences observed for the conductivities of the coatings with SC Al/Al alloys.

Few studies reported values of electrical conductivity for cold sprayed tin onto CFRP: Che et al. (Ref 45, 48) obtained conductivities around 50% bulk Sn conductivity without annealing in previous studies with Sn-10Cu or Sn-10Zn powder mixtures. In other instances of cold-spray metallization of polymers, Małachowska et al. (Ref 63) reported electrical conductivities around 25% the conductivity of bulk tin when cold spraying on polycarbonates. Therefore, the measured electrical conductivities for the tin coatings in this work (Fig. 12) are higher than those reported in previous studies (50-80%). Post-processing treatments could be proposed to improve coating bonding, and therefore conductivity, as had observed Che et al. when annealing several Sn-Cu coatings (from 50 to 80% the bulk conductivity of tin) (Ref 45).

Conclusions

Coatings of tin mixed with various secondary components were cold sprayed with a CenterLine low-pressure cold-spray system, onto thermosetting epoxy-CFRP substrates with varying surface finishes and a thermoplastic PEEK-CFRP. The pull-off strength of these coatings was studied, and the fracture surfaces were characterized. The results indicate that the strength on the thermosetting CFRPs was better than the strength on the PEEK-CFRP. The mechanisms seem related to the degree of deformation/penetration of tin around the superficial carbon fiber areas for the bare e-CFRP, putty e-CFRP and PEEK-CFRP, while the surface film e-CFRP seems to react to a different

mechanism (related to its surface finish). Correlation between the pull-off strength and the SC properties was possible, and it was observed that the better coating strengths were obtained with SC that were previously reported to be detrimental to pure Sn deposition. These results are in opposition to the pure Sn DE improvement mechanism that relied on low hardness/low impact energy SC to catalyze Sn deposition. Attempts to characterize and correlate pull-off strengths to surface roughness parameters were made on the bare e-CFRP substrates after peeling of the coatings, and while preliminary results seemed promising (i.e., the addition of SC generated more surface roughening), there were no clear trends between the parameters and strength results. Finally, the electrical conductivity of each coated substrate was also measured, yet few trends appeared from the results: the conductivity results were generally better than those previously reported, and while they do not provide insight into the deposition/bonding mechanism, they could be an indication of the bonding of the tin in the coating.

Acknowledgments The authors wish to acknowledge the financial support of the Natural Sciences and Engineering Research Council of Canada (NSERC) through the Green-SEAM strategic network and the McGill Engineering Doctoral Award (MEDA). The industrial partners, Bombardier Aerospace and Tencate (through Pratt and Whitney Canada), are gratefully acknowledged. Mr. Kévin Bricault from National Research Council Canada, Boucherville, is acknowledged for his contribution to the cold-spray experiments. Mrs. Marie-Hélène Bernier from École Polytechnique de Montréal is acknowledged for her support in conducting the electrical conductivity measurements.

References

1. R. Gonzalez, H. Ashrafizadeh, A. Lopera, P. Mertiny and A. McDonald, A Review of Thermal Spray Metallization of Polymer-Based Structures, *J. Therm. Spray Technol.*, 2016, **25**(5), p 897–919.
2. F. Faupel, V. Zaporozhchenko, T. Strunskus, J. Erichsen, K. Dolgner, A. Thran and M. Kiene, Fundamental Aspects of Polymer Metallization, *Metallization of Polymers*, 2nd ed., E. Sacher Ed., Springer, Montréal and Québec, 2002, p 73–96
3. Handbook-Airframe, Aviation Maintenance Technician Vol. 1, US Department of Transportation, Federal Aviation Administration, 2018 (Oklahoma City, OK), p 6-7
4. S. Black, Lightning Strike Protection Strategies for Composite Aircraft, *High-Performance Composites, Composites World*, 2013, **21**(3), p 52–61.
5. J. Siegel and V. Kotál, Preparation of Thin Metal Layers on Polymers, *Acta Polytech.*, 2007, **47**(1), p 9–11.
6. T. Duguet, F. Senocq, L. Laffont and C. Vahlas, Metallization of Polymer Composites by Metalorganic Chemical Vapor Deposition of Cu: Surface Functionalization Driven Films Characteristics, *Surf. Coat. Technol.*, 2013, **230**, p 254–259.
7. S. Kuroda, J. Kawakita, M. Watanabe and H. Katanoda, Warm Spraying – a Novel Coating Process based on High-Velocity Impact of Solid Particles, *Sci. Technol. Adv. Mat.*, 2008, **9**(3), p 033002.

8. G. Archambault, B. Jodoin, S. Gaydos and M. Yandouzi, Metallization of Carbon Fiber Reinforced Polymer Composite by Cold Spray and Lay-Up Molding Processes, *Surf. Coat. Technol.*, 2016, **300**, p 78–86.
9. R. Wang, D. Song, W. Liu and X. He, Effect of Arc Spraying Power on the Microstructure and Mechanical Properties of Zn–Al Coating Deposited onto Carbon Fiber Reinforced Epoxy Composites, *Appl. Surf. Sci.*, 2010, **257**(1), p 203–209.
10. C. Feng, M. Gibbons and S. Chandra, Fabrication of Composite Heat Sinks Consisting of a Thin Metallic Skin and a Polymer Core Using Wire-Arc Spraying, *J. Therm. Spray Technol.*, 2019, **28**(5), p 974–985.
11. S. Devaraj, B. Anand, M. Gibbons, A. McDonald and S. Chandra, Thermal Spray Deposition of Aluminum and Zinc Coatings on Thermoplastics, *Surf. Coat. Technol.*, 2020, **399**, 126114.
12. A. Rezzoug, S. Abdi, A. Kaci and M. Yandouzi, Thermal Spray Metallisation of Carbon Fibre Reinforced Polymer Composites: Effect of Top Surface Modification on Coating Adhesion and Mechanical Properties, *Surf. Coat. Technol.*, 2018, **333**, p 13–23.
13. R. Gonzalez, A. McDonald and P. Mertiny, Effect of Flame-Sprayed Al–12Si Coatings on the Failure Behaviour of Pressurized Fibre-Reinforced Composite Tubes, *Polym. Test.*, 2013, **32**(8), p 1522–1528.
14. S. Guan hong, H. Xiaodong, J. Jiuxing and S. Yue, Parametric Study of Al and Al₂O₃ Ceramic Coatings Deposited by Air Plasma Spray onto Polymer Substrate, *Appl. Surf. Sci.*, 2011, **257**(17), p 7864–7870.
15. W. Huang, X. Fan, Y. Zhao, X. Zhou, X. Meng, Y. Wang, B. Zou, X. Cao and Z. Wang, Fabrication of Thermal Barrier Coatings onto Polyimide Matrix Composites via Air Plasma Spray Process, *Surf. Coat. Technol.*, 2012, **207**, p 421–429.
16. A. Sturgeon, B. Dunn, S. Celotto, and B. O'Neill, Cold Sprayed Coatings for Polymer Composite Substrate, Proceedings of the 10th ISMSE, 8th ICPMSE, on CD-ROM, B. ed by Battrick, June 19-23, (Collioure, France), ESA Publications Division (2006)
17. J. Affi, H. Okazaki, M. Yamada and M. Fukumoto, Fabrication of Aluminum Coating onto CFRP Substrate by Cold Spray, *Mater. Trans.*, 2011, **52**(9), p 1759–1763.
18. V.F. Kosarev, S.V. Klinkov, A.P. Alkhimov and A.N. Papyrin, On Some Aspects of Gas Dynamics of the Cold Spray Process, *J. Therm. Spray Technol.*, 2003, **12**(2), p 265–281.
19. S. Kuroda, M. Watanabe, K. Kim and H. Katanoda, Current Status and Future Prospects of Warm Spray Technology, *J. Therm. Spray Technol.*, 2011, **20**(4), p 653–676.
20. A. Moridi, S.M. Hassani-Gangaraj, M. Guagliano and M. Dao, Cold Spray Coating: Review of Material Systems and Future Perspectives, *Surf. Eng.*, 2014, **30**(6), p 369–395.
21. R.N. Raelison, Y. Xie, T. Sapanathan, M.P. Planche, R. Kromer, S. Costil and C. Langlade, Cold Gas Dynamic Spray Technology: A Comprehensive Review of Processing Conditions for Various Technological Developments Till to Date, *Addit. Manuf.*, 2018, **19**, p 134–159.
22. D. Zhang, P.H. Shipway and D.G. McCartney, Cold Gas Dynamic Spraying of Aluminum: The Role of Substrate Characteristics in Deposit Formation, *J. Therm. Spray Technol.*, 2005, **14**(1), p 109–116.
23. A. Ganesan, M. Yamada and M. Fukumoto, Cold Spray Coating Deposition Mechanism on the Thermoplastic and Thermosetting Polymer Substrates, *J. Therm. Spray Technol.*, 2013, **22**(8), p 1275–1282.
24. H. Che, P. Vo and S. Yue, Metallization of Carbon Fibre Reinforced Polymers by Cold Spray, *Surf. Coat. Technol.*, 2017, **313**, p 236–247.
25. A. Ganesan, J. Affi, M. Yamada and M. Fukumoto, Bonding Behavior Studies of Cold Sprayed Copper Coating on the PVC Polymer Substrate, *Surf. Coat. Technol.*, 2012, **207**, p 262–269.
26. H. Che, X. Chu, P. Vo and S. Yue, Metallization of Various Polymers by Cold Spray, *J. Therm. Spray Technol.*, 2017, **27**(1–2), p 169–178.
27. J. Sun, S. Zhou, K. Yamanaka, Y. Ichikawa, H. Saito, K. Ogawa and A. Chiba, Thermal Effects in Sn Coating on a Carbon Fiber Reinforced Plastic by Cold Spraying, *J. Therm. Spray Technol.*, 2021, **30**(5), p 1254–1261.
28. R. Lupoi and W. O'Neill, Deposition of Metallic Coatings on Polymer Surfaces using Cold Spray, *Surf. Coat. Technol.*, 2010, **205**(7), p 2167–2173.
29. R. Della Gatta, A. Viscusi, A. Serena Perna, A. Caraviello and A. Astarita, Feasibility of Steel Powder Deposition on Composites Through Cold Spray, *Mater. Manuf. Proc.*, 2021, **36**(3), p 281–291.
30. A.S. Perna, A. Astarita, P. Carlone, X. Guthmann and A. Viscusi, Characterization of Cold-Spray Coatings on Fiber-Reinforced Polymers through Nanoindentation Tests, *Metals*, 2021, **11**(2), p 1–16.
31. R. Della Gatta, A. Viscusi, A. Serena Perna, A. Caraviello and A. Astarita, Cold Spray Process for the Production of AlSi10Mg Coatings on Glass Fibers Reinforced Polymers, *Mater Manuf Process*, 2021, **36**(1), p 106–121.
32. A. Viscusi, V. Antonucci, L. Carrino, R. Della Gatta, V. Lopresto, I. Papa, A.S. Perna, M.R. Ricciardi and A. Astarita, Manufacturing of an Innovative Composite Structure: Design, *Manuf. Impact Behav. Compos Struct.*, 2020, **250**, p 112637.
33. V. Gillet, E. Aubignat, S. Costil, B. Courant, C. Langlade, P. Casari, W. Knapp and M.P. Planche, Development of Low Pressure Cold Sprayed Copper Coatings on Carbon Fiber Reinforced Polymer (CFRP), *Surf. Coat. Technol.*, 2019, **364**, p 306–316.
34. L.L. Koithara, R.N. Raelison, S. Costil and X. Xie, High Deposition Efficiency and Delamination Issues during High-Pressure Cold Spraying Metallization of PEEK using Spherical Copper Powders, *Int. J. Adv. Manuf. Tech.*, 2020, **107**(11–12), p 4427–4436.
35. P. Lomonaco, S. Weiller, I. Feki, A. Debray, F. Delloro, M. Jeandin, B. Favini and C. Rossignol, Cold Spray Technology to Promote Conductivity of Short Carbon Fiber Reinforced Polyether-Ether-Ketone (PEEK), *Key Eng. Mat.*, 2019, **813**, p 459–464.
36. M. Gardon, A. Latorre, M. Torrell, S. Dosta, J. Fernández and J.M. Guilemany, Cold Gas Spray Titanium Coatings onto a Biocompatible Polymer, *Mater. Lett.*, 2013, **106**, p 97–99.
37. E. Irissou, J.-G. Legoux, B. Arsenault and C. Moreau, Investigation of Al–Al₂O₃ Cold Spray Coating Formation and Properties, *J. Therm. Spray Technol.*, 2007, **16**(5–6), p 661–668.
38. H. Koivuluoto and P. Vuoristo, Effect of Powder Type and Composition on Structure and Mechanical Properties of Cu + Al₂O₃ Coatings Prepared by using Low-Pressure Cold Spray Process, *J. Therm. Spray Technol.*, 2010, **19**(5), p 1081–1092.
39. H.Y. Lee, Y.H. Yu, Y.C. Lee, Y.P. Hong and K.H. Ko, Cold Spray of SiC and Al₂O₃ With Soft Metal Incorporation: A Technical Contribution, *J. Therm. Spray Technol.*, 2004, **13**(2), p 184–189.
40. X.-T. Luo, Y.-K. Wei, Y. Wang and C.-J. Li, Microstructure and Mechanical Property of Ti and Ti6Al4V Prepared by an In-Situ Shot Peening Assisted Cold Spraying, *Mater. Design*, 2015, **85**, p 527–533.
41. Y.-K. Wei, Y.-J. Li, Y. Zhang, X.-T. Luo and C.-J. Li, Corrosion Resistant Nickel Coating with Strong Adhesion on AZ31B Magnesium Alloy Prepared by an In-Situ Shot-Peening-Assisted Cold Spray, *Corros. Sci.*, 2018, **138**, p 105–115.
42. Y.-K. Wei, X.-T. Luo, C.-X. Li and C.-J. Li, Optimization of In-Situ Shot-Peening-Assisted Cold Spraying Parameters for Full Corrosion Protection of Mg Alloy by Fully Dense Al-Based

- Alloy Coating, *J. Therm. Spray Technol.*, 2017, **26**(1–2), p 173–183.
43. R. Fernandez and B. Jodoin, Cold Spray Aluminum-Alumina Cermet Coatings: Effect of Alumina Content, *J. Therm. Spray Technol.*, 2018, **27**(4), p 603–623.
44. R. Fernandez and B. Jodoin, Cold Spray Aluminum-Alumina Cermet Coatings: Effect of Alumina Morphology, *J. Therm. Spray Technol.*, 2019, **28**(4), p 737–755.
45. H. Che, X. Chu, P. Vo and S. Yue, Cold Spray of Mixed Metal Powders on Carbon Fibre Reinforced Polymers, *Surf. Coat. Technol.*, 2017, **329**, p 232–243.
46. A.C. Liberati, H. Che, P. Vo and S. Yue, Influence of Secondary Component Hardness When Cold Spraying Mixed Metal Powders on Carbon Fiber Reinforced Polymers, *J. Therm. Spray Technol.*, 2021, **30**(5), p 1239–1253.
47. A.C. Liberati, H. Che, M. Aghasibeig, K.R. Yu, P. Vo and S. Yue, On the Importance of Secondary Component Properties for Cold Spray Metallization of Carbon Fiber Reinforced Polymers, *J. Therm. Spray Technol.*, 2022, **31**(1–2), p 159–175.
48. H. Che, M. Gagné, P.S.M. Rajesh, J.E. Klemberg-Sapieha, F. Sirois, D. Therriault and S. Yue, Metallization of Carbon Fiber Reinforced Polymers for Lightning Strike Protection, *J. Mater. Eng. Perform.*, 2018, **27**(10), p 5205–5211.
49. H. Che, A.C. Liberati, X. Chu, M. Chen, A. Nobari, P. Vo and S. Yue, Metallization of Polymers by Cold Spraying with Low Melting Point Powders, *Surf. Coat. Technol.*, 2021, **418**, 127229.
50. A. Liberati, H. Che, P. Vo, and S. Yue, Cold Spraying of Mixed Sn-Al Powders onto Carbon Fibre Reinforced Polymers, ITSC (2018) Proceedings of the International Thermal Spray Conference ed by F. Azarmi, K. Balani, T. Eden, T. Hussain, Y.-C. Lau, H. Li, and K. Shinoda, May 7-10, (2018) (ASM International, Orlando, Florida), p 166-172
51. A.C. Liberati, H. Che, P. Vo and S. Yue, Observation of an Indirect Deposition Effect while Cold Spraying Sn-Al Mixed Powders onto Carbon Fiber Reinforced Polymers, *J. Therm. Spray Technol.*, 2020, **29**(1–2), p 134–146.
52. A. Ganesan, M. Yamada and M. Fukumoto, The Effect of CFRP Surface Treatment on the Splat Morphology and Coating Adhesion Strength, *J. Therm. Spray Technol.*, 2013, **23**(1–2), p 236–244.
53. A. Małachowska, M. Winnicki, Ł Konat, T. Piwowarczyk, L. Pawłowski, A. Ambroziak and M. Stachowicz, Possibility of Spraying of Copper Coatings on Polyamide 6 with Low Pressure Cold Spray Method, *Surf. Coat. Technol.*, 2017, **318**, p 82–89.
54. X.L. Zhou, A.F. Chen, J.C. Liu, X.K. Wu and J.S. Zhang, Preparation of Metallic Coatings on Polymer Matrix Composites by Cold Spray, *Surf. Coat. Technol.*, 2011, **206**(1), p 132–136.
55. X. Chu, H. Che, P. Vo, R. Chakrabarty, B. Sun, J. Song and S. Yue, Understanding the Cold Spray Deposition Efficiencies of 316L/Fe Mixed Powders by Performing Splat Tests onto As-Polished Coatings, *Surf. Coat. Technol.*, 2017, **324**, p 353–360.
56. X. Chu, H. Che and S. Yue, Understanding the Cold Spray Deposition Characteristics of Mixed Metal Powders, *MRS Adv.*, 2019, **4**(55–56), p 2989–2995.
57. W. Wong, P. Vo, E. Irissou, A.N. Ryabinin, J.-G. Legoux and S. Yue, Effect of Particle Morphology and Size Distribution on Cold-Sprayed Pure Titanium Coatings, *J. Therm. Spray Technol.*, 2013, **22**(7), p 1140–1153.
58. X. Chu, R. Chakrabarty, H. Che, L. Shang, P. Vo, J. Song and S. Yue, Investigation of the Feedstock Deposition Behavior in a Cold Sprayed 316L/Fe Composite Coating, *Surf. Coat. Technol.*, 2018, **337**, p 53–62.
59. C. Gomez, R. Su, A. Thompson, J. DiSciaccia, S. Lawes and R.K. Leach, Optimization of Surface Measurement for Metal Additive Manufacturing using Coherence Scanning Interferometry, *Opt. Eng.*, 2017, **56**(11), p 111714.
60. Mx Surface Texture Parameters, Zygo, AMETEK Inc, 2018
61. F.M. Smits, Measurement of sheet resistivities with the four-point probe, *Bell Syst. Tech. J.*, 1958, **37**(3), p 711–718.
62. S. Theimer, M. Graunitz, M. Schulze, F. Gaertner and T. Klassen, Optimization Adhesion in Cold Spraying onto Hard Substrates: A Case Study for Brass Coatings, *J. Therm. Spray Technol.*, 2019, **28**(1), p 124–134.
63. A. Małachowska, M. Winnicki, M. Stachowicz and M. Korzeniowski, Metallisation of Polycarbonates using a Low Pressure Cold Spray Method, *Surf. Eng.*, 2018, **34**(3), p 251–258.

Publisher's Note Springer Nature remains neutral with regard to jurisdictional claims in published maps and institutional affiliations.